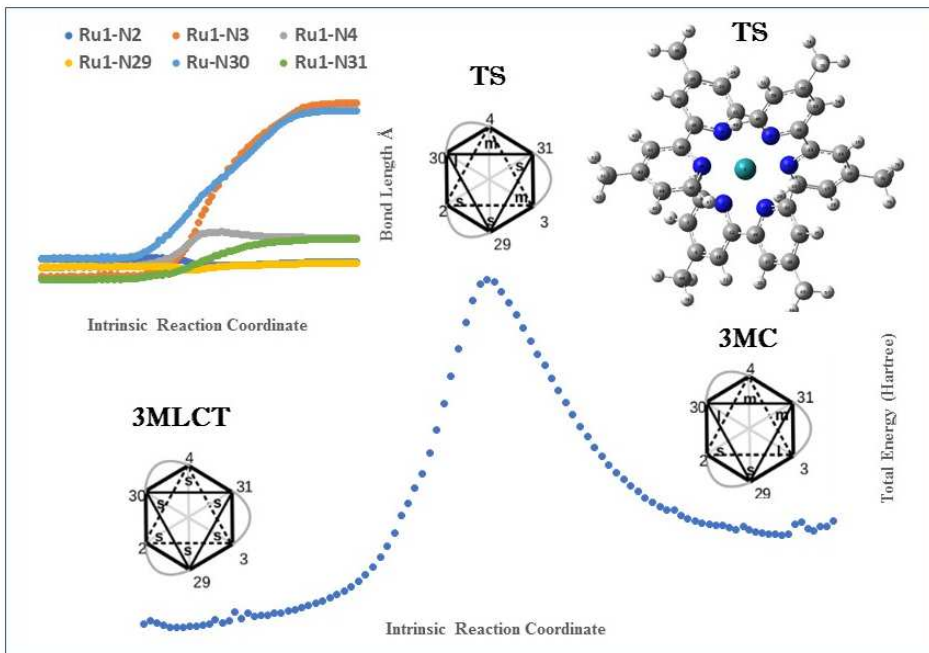


Test of the Orbital-Based LI3 Index as a Predictor of the Height of the $^3\text{MLCT} \rightarrow ^3\text{MC}$ Transition-State Barrier for $[\text{Ru}(\text{N}^{\wedge}\text{N})_3]^{2+}$ Polypyridine Complexes in CH_3CN

Ala Aldin M. H. M. Darghouth*, Denis Magero, and Mark E. Casida

Abstract

Ruthenium(II) polypyridine compounds often have a relatively long-lived triplet metal-ligand charge transfer ($^3\text{MLCT}$) state, making these complexes useful as chromophores for photoactivated electron transfer in photomolecular devices (PMDs). As different PMDs typically require different ligands and as the luminescence lifetime of the $^3\text{MLCT}$ is sensitive to the structure of the ligand, it is important to understand this state and what types of photoprocesses can lead to its quenching. Recent work has increasingly emphasized that there are likely multiple competing pathways involved which should be explored in order to fully comprehend the $^3\text{MLCT}$ state. However the lowest barrier that needs to be crossed to pass over to the nonluminescent triplet metal-centered (^3MC) state has been repeatedly found to be a *trans* dissociation of the complex, at least in the simpler cases studied. This is the fourth in a series of articles investigating the possibility of an orbital-based luminescence index (LI3, because it was the most successful of three) for predicting luminescence lifetimes. In an earlier study of bidentate ($\text{N}^{\wedge}\text{N}$) ligands, we showed that the gas-phase $^3\text{MLCT} \rightarrow ^3\text{MC}$ mechanism proceeded via an initial charge transfer to a single $\text{N}^{\wedge}\text{N}$ ligand which moves symmetrically away from the central ruthenium atom, followed by a bifurcation pathway to one of two ^3MC enantiomers. The actual transition state barrier was quite small and independent, to within the limits of our calculations, to the choice of ligand studied. Here we investigate the same reaction in acetonitrile, CH_3CN , solution and find that the mechanism differs from that in the gas phase in that the reaction passes directly via a *trans* mechanism. This has implications for the interpretation of LI3 via the Bell-Evans-Polanyi principle.



Graphical Abstract

1 Introduction

Polypyridine ruthenium(II) complexes are a class of compounds containing chromophores with a long-lived excited state which can transfer charge to other molecules or within a single large molecule. As such they have elicited, and are expected to continue to elicit, immense interest [1, 2, 3, 4, 5, 6, 7, 8, 9, 10, 11, 12, 13]. A central question has been what features of the ligands favor long luminescence lifetimes and answers are, at least informally, discussed within the context of ligand field theory (LFT). This suggests that we should be able to understand luminescence lifetimes not just from states but also, at least partially, from orbital information. This orbital \leftrightarrow luminescence lifetime connection is gradually being elucidated in a series of articles, of which this is the fourth. The first article (hereafter referred to as **I**) showed how the partial density of states (PDOS) obtained from gas-phase density-functional theory (DFT) calculations could be used to define a LFT-like decomposition of the electronic structure of polypyridine ruthenium(II) complexes [14]. In particular, the energies ϵ of the ruthenium t_{2g} , e_g^* , and ligand π^* orbitals could be determined with reasonable precision. Article **II** analyzed data for roughly one hundred compounds and found that an orbital-based luminescence index (LI) of which the third one,

LFT

PDOS,
DFT

LI, LI3

$$\text{LI3} = \frac{\left[\frac{(\epsilon_{e_g^*} + \epsilon_{\pi^*})}{2} \right]^2}{\epsilon_{e_g^*} - \epsilon_{\pi^*}}. \quad (1)$$

correlated well with trends in experimental luminescence lifetimes as represented by an empirical average triplet metal-ligand-charge-transfer (${}^3\text{MLCT}$) to triplet metal-centered (${}^3\text{MC}$) energy barrier E_{ave} [15]. The LI3 index was based upon frontier-molecular orbital (FMO) theory ideas and designed with the ${}^3\text{MLCT} \rightarrow {}^3\text{MC}$ barrier height in mind but this

${}^3\text{MLCT}$,
 ${}^3\text{MC}$,
 E_{ave}
FMO

was not explicitly verified. Article **III** carried out an investigation of the barrier to *trans* dissociation on the lowest triplet potential energy surface (PES) for the compounds shown in **Fig. 1** for which line drawings are given for the ligands in **Fig. 2** [16]. Calculations in Article **III** were gas-phase calculations using the same functional and basis set as used in Article **II**. It was discovered that LI3 correlates very well with the $^3\text{MLCT}$ - ^3MC energy difference but that finding the transition state (TS) for *trans* dissociation is complicated by the presence of a bifurcation on the PES. This bifurcation is, in part, the result of the diversity of possible Jahn-Teller distortions in octahedral complexes [17] which may give rise to similar competing product geometries [18, 19]. Once this bifurcation is taken into account, barrier heights were found to be very similar for the four compounds investigated. However E_{ave} was derived from condensed phase data and the mechanism of charge transfer reactions can be sensitive to the choice of solvent. It is the objective of the present article to re-investigate LI3 and the *trans* dissociation mechanism on the triplet PES using an implicit solvent model where the solvent has been chosen as the polar solvent acetonitrile (CH_3CN , dielectric constant $\epsilon = 37.5$), very frequently used in experimental work on these complexes. This means that we must reoptimize the singlet ground state (^1GS), extract the PDOS, recalculate LI3, reoptimize the two triplet minima ($^3\text{MLCT}$ and ^3MC), and find the TS and intrinsic reaction coordinate (IRC) linking them for the reaction in acetonitrile.

TS

^1GS ,
IRC

As this article is part of the special “Computational Science from Africa and the African Diaspora,” it seems appropriate to quote a proverb in the national language (Swahili) of the African author (DM):

Haraka haraka haina baraka
Hurry hurry has no blessing.

The relevance of this proverb in the present context lies in the complexity of the problem of understanding luminescence lifetimes in ruthenium(II) polypyridine complexes. These complexes begin in a d^6 ^1GS which may be photoexcited to higher-lying states, notably singlet metal-ligand charge-transfer ($^1\text{MLCT}$) states which is believed to decay rapidly via radiationless relaxation to the lowest $^1\text{MLCT}$ state is then quickly transformed to the phosphorescent $^3\text{MLCT}$ state through intersystem crossing due to the heavy atom effect. The luminescence of this $^3\text{MLCT}$ state is believed to be quenched by radiationless relaxation to other states, notably by passing over a barrier to a ^3MC state, thereby leading to an *increase* in the rapidity of the disappearance of the luminescent state and hence to a *shorter* luminescence lifetime. This ^3MC state is thought to further relax to the ^1GS via another intersystem crossing. In reality, there is probably not a single $^3\text{MLCT} \rightarrow ^3\text{MC} \rightarrow ^1\text{GS}$ pathway, but rather many such pathways. This is especially evident for heteroleptic complexes as different ligands may undergo partial $^3\text{MLCT} \rightarrow ^3\text{MC}$ dissociation. However even in homoleptic complexes, such as the ones treated in this article, different types of $^3\text{MLCT} \rightarrow ^3\text{MC}$ dissociation are possible. In their recent review article [13], Hernández, Eder, and González summarize the literature by grouping luminescence mechanism proposals into three types and then adding a fourth type. Type I says that the rate of luminescence quenching is determined solely by the $^3\text{MLCT}$ - ^3MC energy difference. Type II says that the rate of luminescence quenching is determined by the $^3\text{MLCT} \rightarrow ^3\text{MC}$ barrier. Type III takes into account the barriers for all three of the processes $^3\text{MLCT} \rightarrow ^3\text{MC}$, $^3\text{MC} \rightarrow ^3\text{MLCT}$, and $^3\text{MC} \rightarrow ^1\text{GS}$. To this we may add a fourth type (type IV), as this is the subject of the Hernández-Eder-González article,

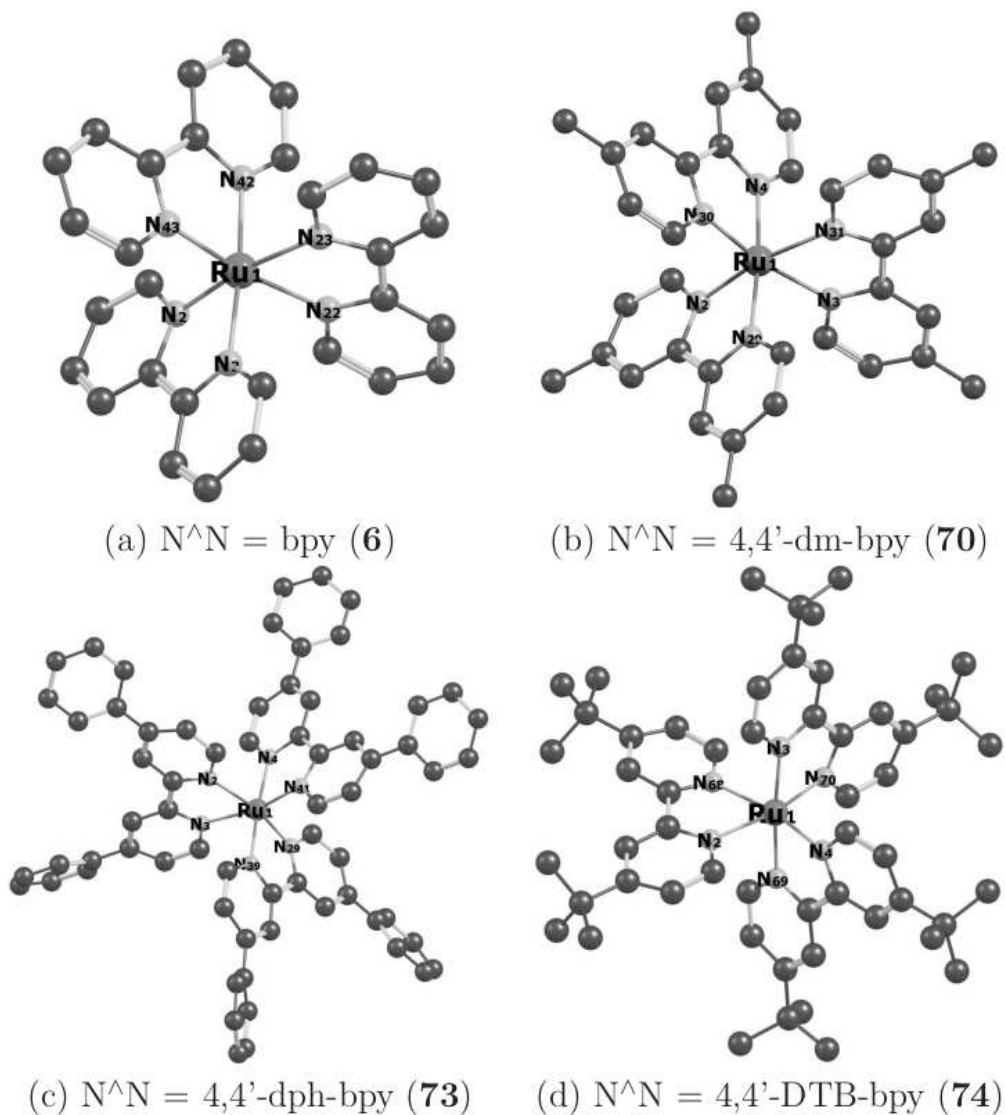
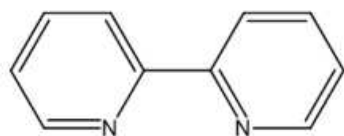
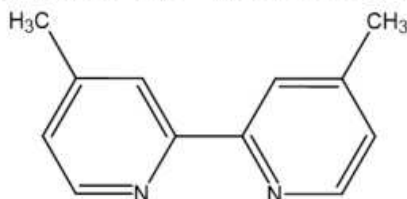


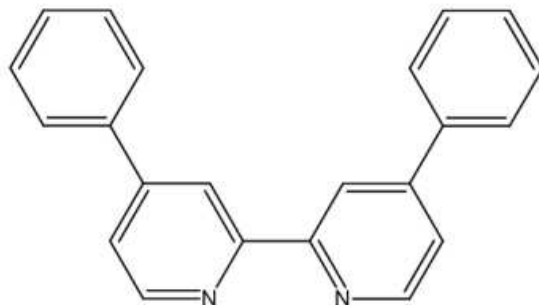
Figure 1: Structures of $[\text{Ru}(N^N)_3]^{2+}$. Hydrogen atoms have been suppressed for clarity. We have chosen to use the Δ stereoisomers, though similar results are expected for the corresponding Λ stereoisomers. Reproduced from Ref. [16].



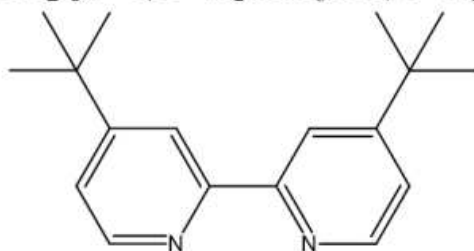
(a) **bpy**: 2,2'-bipyridine (**6**)



(b) **4,4'-dm-bpy**: 4,4'-dimethyl-2,2'-bipyridine (**70**)



(c) **4,4'-dph-bpy**: 4,4'-diphenyl-2,2'-bipyridine (**73**)



(d) **4,4'-DTB-bpy**: 4,4'-di-tert-butyl-2,2'-bipyridine (**74**)

Figure 2: Ligand list. Reproduced from Ref. [16].

which acknowledges that there are several different ^3MC states and that all of these states must be taken into consideration in order to obtain a satisfactory theory. However, the Hernández-Eder-González theory is based upon Eyring’s transition state theory which represents one limit of dynamical theory, Marcus theory being yet another limit, and even the concept of temperature for photochemical reactions in excited states is open to question. In this sense, we find it interesting that one theoretical study of $[\text{Ru}(\text{bpy})_3]^{2+}$ in solution implied that charge is not transferred to a single ligand but rather to two ligands at a time [20] while another article suggests the importance of studying the volume of the various TSs and ^3MC basins based upon a theoretical exploration of the photodynamics of rhodium(III) photosensitizers [18]. Nevertheless, we applaud the Hernández-Eder-González article and willingly acknowledge that the LI3 index proposed in Article **II** is a type II theory which happens to fit trends derived from experiments on around 100 complexes fairly well. But that our reasoning was indirect and not entirely satisfactory. This led us to a further gas-phase theoretical investigation (Article **III**) which appears to favor LI3 as a type I theory. However the experimentally-derived rates used to develop LI3 were based upon condensed phase data. This brings us to the present article where we still consider only the ^3MC state resulting from *trans* partial dissociation according to old rules given by Adamson for photodissociation of O_h complexes [21]. As “hurry has no blessing,” we slow down and make sure that we understand what our orbital-based luminescence index, LI3, is really telling us about the the Adamson mechanism in solution before thinking about where we might go when all the complexities of a type IV theory are taken into account.

The rest of this paper is organized as follows: Our computational methods are described in the next section (Sec. 2). Section 3 presents the results of our computational investigation. Section 4 contains our concluding discussion. Additional information is available as Supplementary Information (SI) (Sec. 4).

SI

2 Methods

Our use of software was dictated not only by what was available to us, but also, in part, by which author was most comfortable with which software. It was thus important to verify that all the software gave (nearly) identical answers. AMHMD carried out calculations with version G09 revision D.01 of GAUSSIAN [22] while DM carried out calculations with version 5.0.4 of ORCA [23]. As reproducibility is also a cornerstone of the scientific method, we also wished to know just how were results obtained using the same method in the two programs. Of course, some differences are expected between different programs using the same method just because of, for example, different convergence criteria, different grids, and different ways to construct solvent accessible volumes, but these are hopefully minor.

In Article **III**, we addressed the problem of being able to carryout the same calculation with ORCA as we had done in Articles **I** and **II** with GAUSSIAN. It turned out that specifying specifying the B3LYP [24] functional does not mean the same thing in the two programs. When the VWN parameterization of the local density approximation was programmed in GAUSSIAN, the VWN parameterization of the random phase approximation (which we shall refer to as VWN3) was used even though this was not the original recommendation of Vosko, Wilke, and Nusair [25]. Instead, these authors recommended their parameterization (which we shall refer to as VWN5) of the quantum Monte Carlo results of Ceperley and Alder. Up until GAUSSIAN used VWN for VWN3, VWN in the literature

VWN3,
VWN5

generally meant VWN5. Moreover the original B3LYP functional programmed in GAUSSIAN uses the VWN3 parameterization, so we will call it B3LYP(VWN3) for clarity. Later some programs redefined B3LYP as B3LYP(VWN5). For example, B3LYP in ORCA is B3LYP(VWN5) but the keyword B3LYP/G allows ORCA users to use B3LYP(VWN3). We also used the ORCA keywords `NORI` (no resolution-of-the-identity approximation is used), `TIGHTSCF`, `TIGHTOPT`, `SLOWCONV`, `NUMFREQ` and an ultra-fine grid. This was explicitly verified in Article **III** where ORCA nudged elastic band (NEB) calculations were carried out using the B3LYP(VWN3) and the resultant NEB first estimate of the intrinsic reaction coordinate (IRC) was subsequently refined using GAUSSIAN [16].

B3LYP(VWN3)
B3LYP(VWN5)

NEB,
IRC

Articles **I-III** are only concerned about gas-phase calculations. However the present article is specifically concerned with if and how our earlier conclusions obtained from gas-phase calculations will need to be changed within an implicit solvent model [26, 27, 28]. In particular, we are interested in the SMD (for Solvation Model based upon the quantum mechanical Density) for our implicit solvent model calculations [29] as this was used in the the NEB ORCA calculations carried out by the Toulouse group [30] (See also Refs [31, 32, 30, 33, 11]).

SMD

To this end, we chose one geometry of complex **6** ($[\text{Ru}(\text{bpy})_3]^{2+}$) and tried to reproduce the same single point energies with ORCA and GAUSSIAN at a variety of computational levels. In particular, we explored the use of two different orbital basis sets and ruthenium effective core potentials (ECPs), namely the 6-31G basis set [34, 35] combined with the LANL2DZ ECP on ruthenium [36] and the larger def2-TZVP [37] basis set combined with the Stuttgart SD28 ECP [38, 39]. We also wished to include Grimme's D3 dispersion correction [40] with Becke-Johnson damping [41].

ECP

The keywords needed to do these calculations differ significantly between ORCA and GAUSSIAN. For example, setting `EmpiricalDispersion=D3` in GAUSSIAN indicates to use Grimme's original D3 dispersion correction [40]. The corresponding keyword in ORCA is `D3ZERO`. Setting `EmpiricalDispersion=GD3BJ` in GAUSSIAN indicates to use the Grimme's semiempirical D3 dispersion correction but with Becke-Johnson damping [41]. The corresponding keyword in ORCA is `D3BJ`. It is also possible for GAUSSIAN users to use B3LYP(VWN5) but the procedure is more delicate and requires the following lines of input [42]. We also discovered that the `SDD` keyword in GAUSSIAN gives the Stuttgart SD28 ECP but uses a different orbital basis set, so that the def2-TZVP for ruthenium needs to be made an explicit part of the input. Thus, in order to do a B3LYP(VWN5)+D3BJ/def2-TZVP & Ru(SD28) calculation we used the following GAUSSIAN input:

```
#p  bv5lyp/gen nosymm  pseudo=read scrf=(solvent=acetonitrile,SMD)  \\  
gfinput pop=full iop(3/76=1000002000) iop(3/77=0720008000)  \\  
iop(3/78=0810010000) EmpiricalDispersion=GD3BJ
```

...

```
N C H  
Def2TZVP  
*****  
Ru  
Def2TZVP  
*****
```

Note that the backslashes here are just to indicate that the entry is all on a single line and the “...” indicates the parts of the input have been removed for brevity. The results are shown in the SI. The largest gas-phase error in the total energy is 67.5 μ Ha (0.0424 kcal/mol) which is acceptable for the present work.

Of course our main interest in the present paper is if and how our earlier gas-phase conclusions will need to be changed in the light of SMD implicit solvent model calculations. Both GAUSSIAN and ORCA have implemented this method in a nearly identical way with gaussian charges, rather than point charges. However they differ in the construction of the solvent accessible region. In particular, GAUSSIAN does an integral-equation-formalism (IEF) point charge continuum model (PCM) calculation [43, 44, 45, 46] while ORCA does a conductor-like polarizable continuum (C-PCM) [47, 48, 49, 50, 51, 52, 53] calculation. A table in the SI indicates a difference in total energies between GAUSSIAN and ORCA calculations of as much as 600 μ Ha (0.377 kcal/mol) which might be compared with the maximum error of 0.5 kcal/mol (796 μ Ha) for solvation energies quoted for differences between the IEF-PCM and C-PCM implementations of the SMD quoted at the top of the second column on page 6390 of Ref. [29]. However a maximum error of less than 0.2 kcal/mol (318 μ Ha) is claimed for ions in a solvent with dielectric constant greater than 32 which is the case for acetonitrile (CH_3CN , $\epsilon \approx 35$). This difference between the SMD calculations in the two programs turns out to be controllable by varying the fineness of the Lebedev grid used in ORCA. The precise keywords to use are

IEF,
PCM,
C-PCM

```
%cpcm  
num_leb X  
end
```

where X is the number of Lebedev grid points per cavity sphere. The default is 110 in version 5 of ORCA but a table in the SI shows that the difference between GAUSSIAN and ORCA calculations may be considerably reduced by using a finer Lebedev grid. We have therefore chosen to use a 590 point Lebedev grid in all our SMD calculations with ORCA unless otherwise specified. Of course, a comparison of energy differences calculated with GAUSSIAN with the same energy differences calculated with ORCA may even be smaller than our observed difference in total energies as error cancellation is common when calculating energy differences.

A question that could be asked, but which is beyond the scope of this article, is to what extent the solvent model needs to be modified to handle excited states which are typically more diffuse and charged solutes, notably the $^3\text{MLCT}$ state where the positive charge is expected to be delocalized onto the ligands rather localized on the ruthenium atom and shielded by the ligands as in the ^3MC state? This, of course, is a question which is general when using any implicit solvent model to treat excited states in solution, with the case of a “solvated” electron, such as when carrying out Birch reduction with sodium in liquid ammonia, as a worst case scenario. We are not aware of it having been as yet much much discussed in the literature.

We carried out calculations at the following levels using the SMD implicit solvent model [29] and corresponding parameters for acetonitrile (CH_3CN):

1. B3LYP(VWN3)/6-31G [34, 35] & LANL2DZ(Ru) [36]/SMD(CH_3CN): Ground state geometries, partial density of states (PDOS), luminescence index (LI), optimized

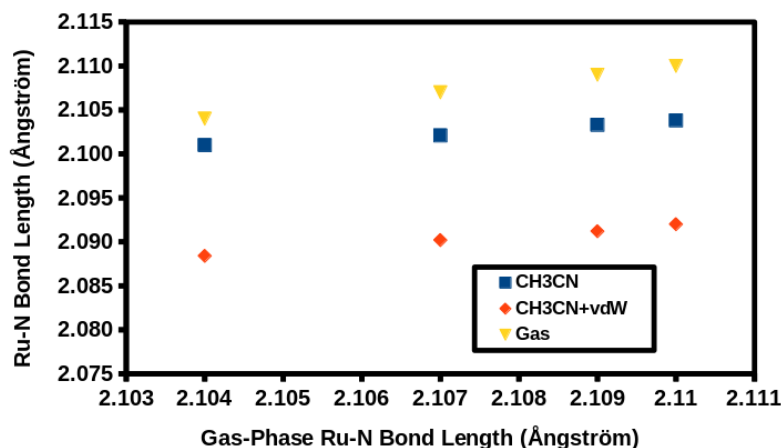


Figure 3: Ground state average Ru-N bond lengths: “Gas,” B3LYP(VWN3)/6-31G & LANL2DZ(Ru) (from [16]); “CH3CN,” B3LYP(VWN3)/6-31G & LANL2DZ(Ru)/SMD(CH₃CN); “CH3CN+vdW,” B3LYP(VWN3)+D3BJ/6-311G(d,p) & LANL2DZ(Ru)/SMD(CH₃CN).

³MLCT and ³MC minima for all 4 complexes (**6**, **70**, **73**, and **74**) and NEB calculations for complexes **6**, **70**, and **73** as well as IRC calculations for complexes **6** and **70**.

- B3LYP(VWN3)+D3BJ/6-31G & LANL2DZ(Ru)/SMD(CH₃CN): Ground state geometries, partial density of states (PDOS), luminescence index (LI), for all 4 complexes (**6**, **70**, **73**, and **74**).
- B3LYP(VWN3), 6-311G(d,p)=6-311G** [54] & LANL2DZ(Ru)/SMD(CH₃CN): Optimized ³MLCT and ³MC minima for complexes **73** and **74**.
- B3LYP(VWN3)+D3BJ/6-311G(d,p)=6-311G** [54] & LANL2DZ(Ru)/SMD(CH₃CN)/SMD(CH₃CN): Ground state geometries, partial density of states (PDOS), luminescence index (LI), for all 4 complexes (**6**, **70**, **73**, and **74**).

3 Results and Discussion

3.1 Ground State Geometries, PDOS, and LI3

Calculations at the B3LYP(VWN3)/6-31G & LANL2DZ(Ru)/SMD(CH₃CN) and B3LYP(VWN3)+D3BJ/6-311G(d,p)& LANL2DZ(Ru)/SMD(CH₃CN) levels are compared with gas-phase B3LYP(VWN3)/6-31G & LANL2DZ(Ru) from Article **III**. As expected for a closed-shell symmetric molecule, the six ground state Ru-N bond lengths within each complex are essentially identical. **Figure 3** shows that the complex contracts slightly in going from the gas-phase to the condensed phase (“chemical pressure” [55]). An even larger compression results when the D3BJ (van der Waals, vdW) dispersion correction is included.

The PDOS for complex **70** is shown in **Fig. 4** while the PDOSs for the other complexes have been relegated to the SI. **Table 1** give the HOMO and PDOS orbital energies in

vdW

HOMO	PDOS Energies		
	t_{2g}	$1\pi^*$	e_g^*
Compound 6			
B3LYP(VWN3)/6-31G & LANL2DZ(Ru) gas phase			
-11.20 eV	-11.06 eV	-7.42 eV	-5.01 eV
B3LYP(VWN3)/6-31G & LANL2DZ(Ru)/SMD(CH ₃ CN)			
-5.645 eV	-5.805 eV	-2.188 eV	+0.285 eV
B3LYP(VWN3)+D3BJ/6-311G(d,p) & LANL2DZ(Ru)/SMD(CH ₃ CN)			
-5.864 eV	-6.022 eV	-2.339 eV	+0.059 eV
Compound 70			
B3LYP(VWN3)/6-31G & LANL2DZ(Ru) gas phase			
-10.42 eV	-10.55 eV	-7.00 eV	-4.53 eV
B3LYP(VWN3)/6-31G & LANL2DZ(Ru)/SMD(CH ₃ CN)			
-5.470 eV	-5.617 eV	-2.078 eV	+0.356 eV
B3LYP(VWN3)+D3BJ/6-311G(d,p) & LANL2DZ(Ru)/SMD(CH ₃ CN)			
-5.679 eV	-5.850 eV	-2.277 eV	+0.083 eV
Compound 73			
B3LYP(VWN3)/6-31G & LANL2DZ(Ru) gas phase			
-9.84 eV	-9.88 eV	-6.53 eV	-4.04 eV
B3LYP(VWN3)/6-31G & LANL2DZ(Ru)/SMD(CH ₃ CN)			
-5.571 eV	-5.678 eV	-2.267 eV	+0.370 eV
B3LYP(VWN3)+D3BJ/6-311G(d,p) & LANL2DZ(Ru)/SMD(CH ₃ CN)			
-5.805 eV	-5.896 eV	-2.519 eV	+0.074 eV
Compound 74			
B3LYP(VWN3)/6-31G & LANL2DZ(Ru) gas phase			
-10.08 eV	-10.20 eV	-6.61 eV	-4.19 eV
B3LYP(VWN3)/6-31G & LANL2DZ(Ru)/SMD(CH ₃ CN)			
-5.464 eV	-5.600 eV	-2.050 eV	+0.420 eV
B3LYP(VWN3)+D3BJ/6-311G(d,p) & LANL2DZ(Ru)/SMD(CH ₃ CN)			
-5.666 eV	-5.831 eV	-2.224 eV	+0.166 eV

Table 1: HOMO and PDOS orbital energies.

Method	$\Delta_{\text{PDOS-LFT}}$	Ru-N Bond Length
Compound 6		
B3LYP(VWN3)/6-31G&LANL2DZ(Ru) gas phase ^a	48,800 cm ⁻¹	2.110 Å
B3LYP(VWN3)/6-31G&LANL2DZ(Ru)/SMD(CH ₃ CN)	49,120 cm ⁻¹	2.1038(4) Å
B3LYP(VWN3)+D3BJ/6-311G(d,p)&LANL2DZ(Ru)/SMD(CH ₃ CN)	49,050 cm ⁻¹	2.0920(1) Å
Compound 70		
B3LYP(VWN3)/6-31G&LANL2DZ(Ru) gas phase ^a	48,600 cm ⁻¹	2.109 Å
B3LYP(VWN3)/6-31G&LANL2DZ(Ru)/SMD(CH ₃ CN)	48,180 cm ⁻¹	2.1033(4) Å
B3LYP(VWN3)+D3BJ/6-311G(d,p)&LANL2DZ(Ru)/SMD(CH ₃ CN)	47,850 cm ⁻¹	2.0912(3) Å
Compound 73		
B3LYP(VWN3)/6-31G&LANL2DZ(Ru) gas phase ^a	47,100 cm ⁻¹	2.104 Å
B3LYP(VWN3)/6-31G&LANL2DZ(Ru)/SMD(CH ₃ CN)	48,780 cm ⁻¹	2.1010(6) Å
B3LYP(VWN3)+D3BJ/6-311G(d,p)&LANL2DZ(Ru)/SMD(CH ₃ CN)	48,150 cm ⁻¹	2.0884(6) Å
Compound 74		
B3LYP(VWN3)/6-31G&LANL2DZ(Ru) gas phase ^a	48,500 cm ⁻¹	2.107 Å
B3LYP(VWN3)/6-31G&LANL2DZ(Ru)/SMD(CH ₃ CN)	48,550 cm ⁻¹	2.1021(13) Å
B3LYP(VWN3)+D3BJ/6-311G(d,p)&LANL2DZ(Ru)/SMD(CH ₃ CN)	48,370 cm ⁻¹	2.0902(17) Å

^aFrom Ref. [15].

Table 2: PDOS-LFT splittings and average Ru-N bond lengths.

the gas phase and with the SMD implicit solvation model. Solvation leads to a significant increase in orbital energies but there is remarkably little change in orbital energy differences upon introduction of solvent effects or solvent effects plus dispersion corrections as shown in **Fig. 5**. **Table 2** shows that the order of the average Ru-N bond lengths is model independent [R(Ru-N): **73** < **74** < **70** < **6**]. It is therefore normal to expect that the PDOS LFT splitting $\Delta_{\text{PDOS LFT}}$ should also vary in the order **73** > **74** > **70** > **6**. The fact that we do not really see this is most likely due to our inability to calculate $\Delta_{\text{PDOS LFT}}$ with sufficient precision.

Let us turn to a modified orbital-based luminescence index LI4 shown in **Table 3**. Our observation that the PDOS in solution is just shifted with respect to the PDOS in the gas phase suggests that Eq. (1) should be modified to include an energy zero ϵ_0 ,

$$\text{LI4} = \frac{\left(\frac{\epsilon_{e_g^*} + \epsilon_{\pi^*}}{2} - \epsilon_0\right)^2}{\epsilon_{e_g^*} - \epsilon_{\pi^*}}. \quad (2)$$

Unfortunately different choices of ϵ_0 will give different results. This is because LI3 was motivated by frontier molecular orbital which depend upon the use of the Wolfsberg-Helmholz approximation [56], albeit with the additional assumption that the overlap integral is unity. Since the Wolfsberg-Helmholz formula has a dependence on the energy zero, so does LI3. Normally the Wolfsberg-Helmholz formula is used in extended Hückel theory where it is used to calculate matrix elements from gas-phase ionization potentials. This might be an argument to explain why LI3 constructed from gas-phase data seemed to work well for estimating trends in (condensed phase) luminescence lifetimes (Article **II**). We have tried different seemingly logical choices of ϵ_0 in Eq. (2) and finally concluded

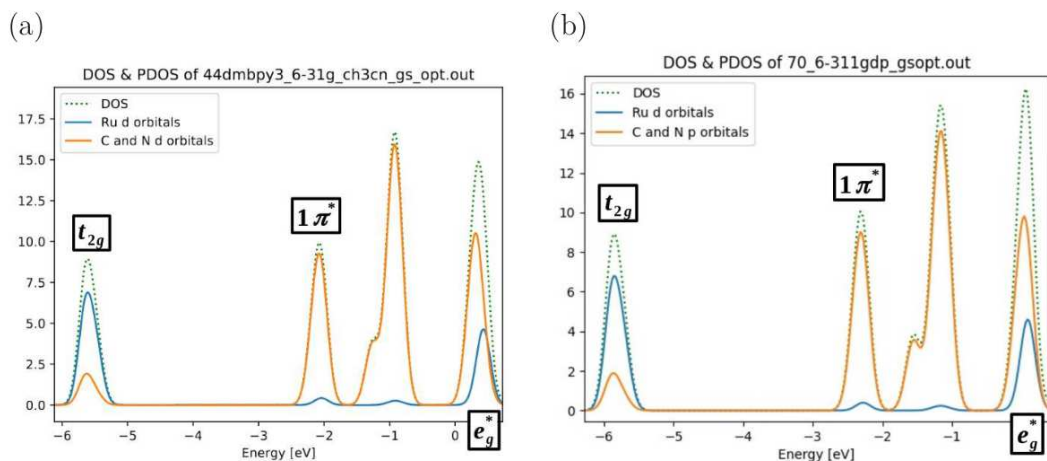


Figure 4: PDOS for complex **70** calculated with 40,000 points and FWHM = 0.25 eV: (a) B3LYP(VWN3)/6-31G & LANL2DZ(Ru)/SMD(CH₃CN), (b) B3LYP(VWN3)+D3BJ/6-311G(d,p) & LANL2DZ(Ru)/SMD(CH₃CN). The corresponding gas-phase B3LYP(VWN3)/6-31G & LANL2DZ(Ru) gas phase PDOS may be found in Ref. [15].

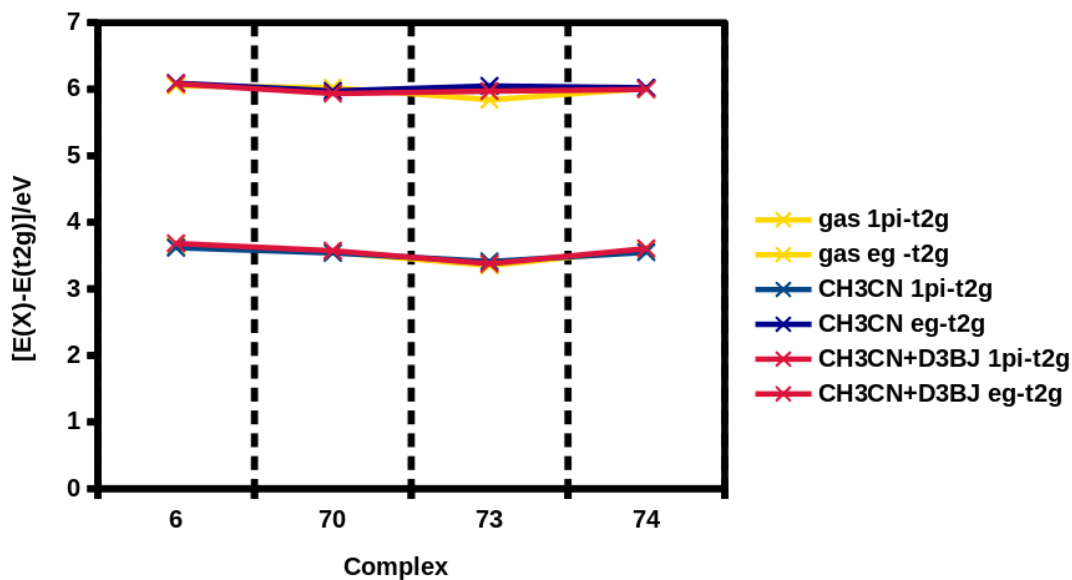


Figure 5: Scaled PDOS orbital energies for all four complexes relative to the t_{2g} energy at each level of modeling: “gas,” B3LYP(VWN3)/6-31G & LANL2DZ(Ru) (from [16]); “CH₃CN,” B3LYP(VWN3)/6-31G & LANL2DZ(Ru)/SMD(CH₃CN); “CH₃CN+D3BJ,” B3LYP(VWN3)+D3BJ/6-311G(d,p) & LANL2DZ(Ru)/SMD(CH₃CN).

LI4			
6	70	73	74
E_{ave}^a			
132 cm ⁻¹	157 cm ⁻¹	94 cm ⁻¹	110 cm ⁻¹
B3LYP(VWN3)/6-31G & LANLDZ(Ru) gas phase ^b			
16.03 eV	13.46 eV	11.21 eV	12.05 eV
B3LYP(VWN3)/6-31G & LANLDZ(Ru)/SMD(CH ₃ CN)			
17.12 eV	13.87 eV	10.32 eV	11.94 eV
B3LYP(VWN3)+D3BJ/6-311G(d,p) & LANLDZ(Ru)/SMD(CH ₃ CN)			
17.49 eV	13.93 eV	10.66 eV	12.40 eV

^aTables 10 and 11 of Ref. [15].

^bFrom Ref. [15].

Table 3: Values of LI4 calculated with different functionals and basis sets in gas phase and in CH₃CN.

that the best choice is,

$$\epsilon_0 = \epsilon_{\text{solvated}}^{\text{HOMO}} - \epsilon_{\text{gas phase}}^{\text{HOMO}}, \quad (3)$$

which shifts the energies calculated in solvent to be close to those calculated in the gas phase. This finishes the definition of LI4, as calculated and tabulated in Table 3. **Figure 6** shows that this definition gives very similar results at all levels of calculation and correlated reasonably well with the quantity E_{ave} derived from experimental data in Article **II**.

3.2 ³MLCT and ³MC Minima

NEB and IRC calculations for the *trans* ³MLCT → ³MC dissociation mechanism require us to optimize the initial ³MLCT reactant and final ³MC product geometries. Optimization of the ³MLCT minimum is relatively straightforward. It suffices to do a vertical excitation from the optimized ground state geometry and then to allow the molecule to relax on the triplet surface. This gives a Jahn-Teller distorted geometry with three pairs of bond lengths, all nearly identical to each other and which we will designate as short.

Finding the ³MC minimum for *trans* dissociation is more difficult. We proceed by a 2D scan where each of the two *trans* bond lengths are varied and the geometry is otherwise fully relaxed. **Figure 7** shows such a scan for complex **70**. Similar plots for complexes **6**, **73**, and **74** may be found in the SI. Note that the scan should be symmetric upon the reflection through, respectively, the Ru1-N22 = Ru1-N43 and R1-N3 = Ru-N30 lines, but only if the same scan minima are found on both sides of the line, which is not expected to happen. However such scans are good enough to allow us to locate a good guess for the ³MC *trans* minimum which is then optimized to give us our final ³MC geometry. As these scans are computationally intensive, we have only done them at the B3LYP(VWN3)/6-31G & LANLDZ(Ru)/SMD(CH₃CN) level for the solvation model. Indeed, this level is our main workhorse, but we have also carried out a few higher-level calculations. Bond length information at this level has been collected in **Table 4**. Notice that the optimized ³MC has two long (l) bonds *trans* to each other, two short (s) bonds, and two medium (m) length bonds. Some ORCA optimized bond lengths have been given to show the level

s, m, l

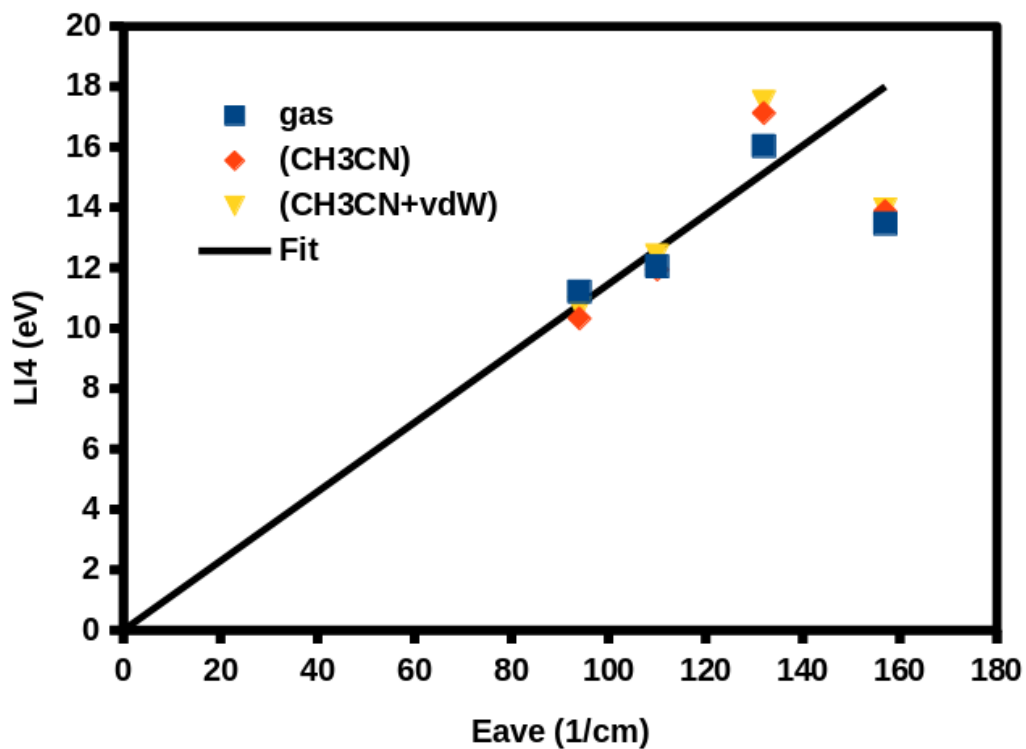


Figure 6: Correlation of LI4 calculated using different levels of modeling with E_{ave} from Article II: “gas,” B3LYP(VWN3)/6-31G & LANL2DZ(Ru) (from [16]); “(CH3CN),” B3LYP(VWN3)/6-31G & LANL2DZ(Ru)/SMD(CH₃CN); “(CH3CN+vdW),” B3LYP(VWN3)+D3BJ/6-311G(d,p) & LANL2DZ(Ru)/SMD(CH₃CN).

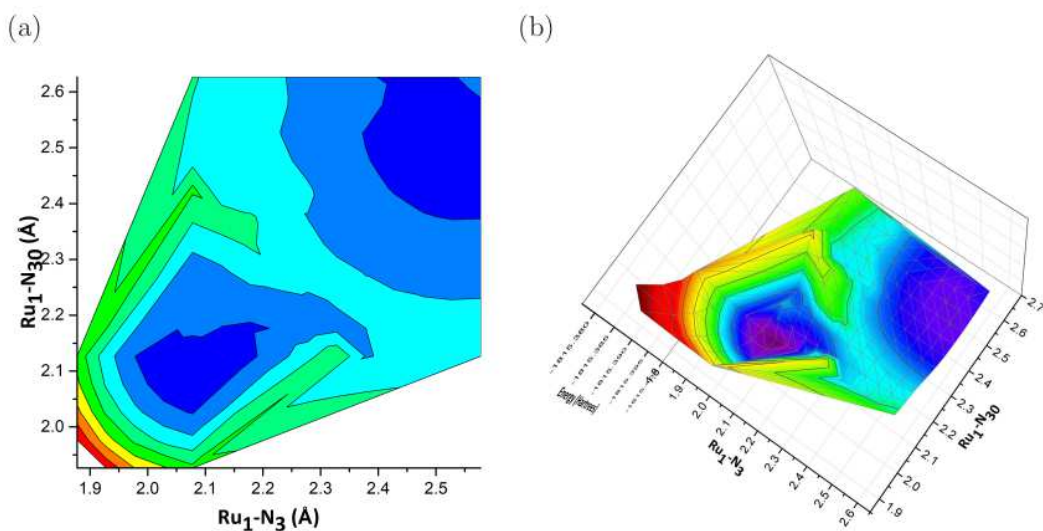


Figure 7: 2D scan for complex **70** using GAUSSIAN at the B3LYP(VWN3)/6-31G & LANL2DZ(Ru)/SMD(CH₃CN) level: (a) contour plot, (b) surface.

of agreement between our ORCA and GAUSSIAN calculations.

For complexes **73** and **74**, we also have optimized geometries at the B3LYP(VWN3)/6-31G(d,p) & LANL2DZ(Ru)/SMD(CH₃CN) (**Table 5**) level.

3.3 ³TS and IRC

TS and IRC calculations are notoriously difficult for ruthenium(II) polypyridine complexes. One reason for this is that there are many different reactions which can occur and the corresponding TSs are not necessarily very far apart. An example was reported in Article **III**, namely that the reaction pathway was complicated by the presence of bifurcations. This is why it is important to have a systematic way to search for the desired IRCs and TSs.

We follow the same procedure as previously described in Article **III**. Briefly, having found the ³MLCT and ³MC minima (step 1), we carry out a NEB calculation with ORCA (step 2). This gives us a first guess as to the ³TS in the form of the ³MEP along the NEB. This ³MEP is only a first approximation to the ³TS. So ORCA further optimizes the ³MEP to give a ³TS. At this point, simply because of the way expertise is distributed among different team members, calculations are continued with GAUSSIAN and the ³TS is reoptimized (step 3). The nature of the TS is confirmed by calculation of vibrational frequencies and making sure that there is a single imaginary vibrational frequency, but this is not enough. The IRC of the ³TS is further calculated with GAUSSIAN to ensure that it leads to the same ³MLCT and ³MC geometries as initially used to generate the NEB (step 4). We also need some way to characterize the pathway. Naturally, this can be done in many different ways (we used more than one!), but we have found that the most useful summary of the pathway is provided by tracing how the six Ru-N bond lengths vary along the IRC (step 5).

Calculations are only reported at the basic B3LYP(VWN3)/6-31G & LANL2DZ(Ru)/SMD(CH₃CN) level. Furthermore we were only able to find the ³MEP for complexes **6**, **70**, and **73**, and the ³TS was only confirmed via IRC calculation for complexes **6** and **70**. This is because the SMD implicit solvent calculations are significantly more compute intensive than are gas-phase calculations. Furthermore, the mechanism of the *trans* ³MLCT → ³MC found with the implicit solvent model turns out to be significantly different than that found in our previous gas-phase calculations (Article **III**). Nevertheless, the ³MEP energy is an upper bound of the ³TS energy and trends in ³MEP energies may be expected to be roughly similar to trends in ³TS energies.

Table 6 summarizes key energies and energy differences. Complex **6** is the prototypical luminescent ruthenium(II) bipyridine complex and, as such, has been extensively studied in the literature. In particular, our value of 1 652.64 cm⁻¹ for the ³MLCT → ³MC barrier height at the B3LYP(VWN3)/6-31G & LANL2DZ(Ru)/SMD(CH₃CN) level may be compared with the two previously obtained theoretical values of 1 138 cm⁻¹ [57] and 3 040 cm⁻¹ [30] also in the same solvent and with the experimental value of 3 800 cm⁻¹ [58] in the same solvent. This is a reminder that the accuracy of modern quantum chemical calculations for transition metal complexes is closer to 5 kcal/mol (1 750 cm⁻¹) [59, 60] than to the oft quoted 1 kcal/mol goal for chemical accuracy.

Bond	Ground State	³ MLCT	³ TS	³ MC
[Ru(bpy) ₃] ²⁺ (6)				
Ru ₁ -N ₂	2.104 (s)	2.125 (s) [2.122 (s)]	2.113 (s) [2.110 (s)]	2.120 (s) [2.109 (s)]
Ru ₁ -N ₃	2.104 (s)	2.112 (s) [2.102 (s)]	2.113 (s) [2.102 (s)]	2.122 (s) [2.109 (s)]
Ru ₁ -N ₂₂	2.104 (s)	2.078 (s) [2.072 (s)]	2.200 (m) [2.208 (m)]	2.497 (l) [2.445 (l)]
Ru ₁ -N ₂₃	2.103 (s)	2.082 (s) [2.071 (s)]	2.116 (s) [2.115 (s)]	2.182 (m) [2.162 (m)]
Ru ₁ -N ₄₂	2.103 (s)	2.113 (s) [2.102 (s)]	2.191 (m) [2.175 (m)]	2.182 (m) [2.162 (m)]
Ru ₁ -N ₄₃	2.104 (s)	2.135 (s) [2.121 (s)]	2.262 (l) [2.258 (l)]	2.503 (l) [2.623 (l)]
[Ru(4,4'-dm-bpy) ₃] ²⁺ (70)				
Ru ₁ -N ₂	2.103 (s)	2.126 (s) [2.121 (s)]	2.109 (s) [2.109 (s)]	2.121 (s) [2.108 (s)]
Ru ₁ -N ₃	2.104 (s)	2.078 (s) [2.071 (s)]	2.210 (m) [2.210 (m)]	2.488 (l) [2.450 (l)]
Ru ₁ -N ₄	2.103 (s)	2.104 (s) [2.101 (s)]	2.180 (m) [2.180 (m)]	2.175 (m) [2.161 (m)]
Ru ₁ -N ₂₉	2.103 (s)	2.106 (s) [2.100 (s)]	2.100 (s) [2.100 (s)]	2.121 (s) [2.108 (s)]
Ru ₁ -N ₃₀	2.104 (s)	2.127 (s) [2.121 (s)]	2.267 (l) [2.266 (l)]	2.519 (l) [2.448 (l)]
Ru ₁ -N ₃₁	2.103 (s)	2.075 (s) [2.071 (s)]	2.116 (s) [2.116 (s)]	2.176 (m) [2.163 (m)]
[Ru(4,4'-dph-bpy) ₃] ²⁺ (73)				
Ru ₁ -N ₂	2.100 (s)	2.101 (s)		2.489 (l)
Ru ₁ -N ₃	2.101 (s)	2.126 (s)		2.177 (m)
Ru ₁ -N ₄	2.102 (s)	2.075 (s)		2.113 (s)
Ru ₁ -N ₂₉	2.100 (s)	2.102 (s)		2.476 (l)
Ru ₁ -N ₃₉	2.101 (s)	2.123 (s)		2.175 (m)
Ru ₁ -N ₄₁	2.101 (s)	2.073 (s)		2.110 (s)
[Ru(4,4'-DTB-bpy) ₃] ²⁺ (74)				
Ru ₁ -N ₂	2.104 (s)	2.106 (s)		2.534 (l)
Ru ₁ -N ₃	2.102 (s)	2.125 (s)		2.167 (m)
Ru ₁ -N ₄	2.101 (s)	2.073 (s)		2.117 (s)
Ru ₁ -N ₆₈	2.104 (s)	2.126 (s)		2.180 (m)
Ru ₁ -N ₆₉	2.102 (s)	2.077 (s)		2.114 (s)
Ru ₁ -N ₇₀	2.101 (s)	2.102 (s)		2.476 (l)

Table 4: Key Ru-N bond lengths (Å) for different compounds as computed with GAUSSIAN at the B3LYP(VWN3)/6-31G & Ru(LANL2DZ)/SMD(CH₃CN) level. In parentheses: “s” stands for “short” (~ 2.1 Å), “m” for “medium length” (~ 2.2 Å), and “l” for “long” (~ 2.3 Å or longer). A few values computed with ORCA are given in square brackets for comparison purposes.

Bond	Ground State	³ MLCT	³ TS	³ MC
	[Ru(4,4'-dph-bpy) ₃] ²⁺ (73)			
Ru ₁ -N ₂	2.110 (s)	2.112 (s)		2.508 (l)
Ru ₁ -N ₃	2.111 (s)	2.142 (s)		2.200 (m)
Ru ₁ -N ₄	2.111 (s)	2.082 (s)		2.124 (s)
Ru ₁ -N ₂₉	2.110 (s)	2.112 (s)		2.508 (l)
Ru ₁ -N ₃₉	2.110 (s)	2.138 (s)		2.198 (m)
Ru ₁ -N ₄₁	2.111 (s)	2.081 (s)		2.124 (s)
	[Ru(4,4'-DTB-bpy) ₃] ²⁺ (74)			
Ru ₁ -N ₂	2.113 (s)	2.115 (s)		2.511 (l)
Ru ₁ -N ₃	2.111 (s)	2.135 (s)		2.199 (m)
Ru ₁ -N ₄	2.109 (s)	2.079 (s)		2.124 (s)
Ru ₁ -N ₆₈	2.113 (s)	2.139 (s)		2.198 (m)
Ru ₁ -N ₆₉	2.111 (s)	2.084 (s)		2.125 (s)
Ru ₁ -N ₇₀	2.109 (s)	2.111 (s)		2.507 (l)

Table 5: Key Ru-N bond lengths (Å) for different compounds as computed with GAUSSIAN at the B3LYP(VWN3)/6-31G(d,p) & Ru(LANLDZ)/SMD(CH₃CN) level. In parentheses: “s” stands for “short” (~ 2.1 Å), “m” for “medium length” (~ 2.2 Å), and “l” for “long” (~ 2.3 Å or longer).

Energy\Complex	6	70	73	74
LI3 (gas)	16.78 eV	13.78 eV	9.68 eV	11.97 eV
³ MLCT	-1579.52991 Ha	-1815.39834 Ha	-2965.61009 Ha	-2522.856703 Ha
³ MC	-1579.52613 Ha	-1815.39367 Ha	-2965.60302 Ha	-2522.851208 Ha
³ MEP	-1579.52122 Ha	-1815.38845 Ha	-2965.59913 Ha	
³ TS	-1579.52238 Ha	-1815.38962 Ha		
³ MEP- ³ MLCT	0.00869 Ha	0.00989 Ha	0.01096 Ha	
	1907.23 cm ⁻¹	2170.60 cm ⁻¹	2405.44 cm ⁻¹	
³ TS- ³ MLCT	0.00753 Ha	0.00872 Ha		
	1652.64 cm ⁻¹	1913.82 cm ⁻¹		
³ MEP- ³ MC	0.00491 Ha	0.00522 Ha	0.00389 Ha	
	1077.62 cm ⁻¹	1145.66 cm ⁻¹	853.76 cm ⁻¹	
³ TS- ³ MC	0.00374 Ha	0.00405 Ha		
	823.03 cm ⁻¹	888.87 cm ⁻¹		
³ MC- ³ MLCT	0.00375 Ha	0.00467 Ha	0.00707 Ha	0.005495 Ha
	829.61 cm ⁻¹	1024.95 cm ⁻¹	1551.69 cm ⁻¹	1206.01 cm ⁻¹

Table 6: Energies for ³MLCT, ³MC and TS of all four compounds obtained from B3LYP(VWN3)/6-31G & LANL2DZ(Ru)/SMD(CH₃CN) NEB calculations as implemented in the ORCA code.

Nevertheless, we may hope for consistent trends within a given theoretical model chemistry (defined by a fixed functional, basis set, etc.) and hence a qualitatively (even semiquantitatively!) correct description of the key *trans* $^3\text{MLCT} \rightarrow ^3\text{MC}$ mechanism. This mechanism is found to change in the present implicit solvent calculations with respect to what we reported earlier in gas-phase in Article **III**. In our gas-phase calculations, to get from the $^3\text{MLCT}$ minimum to the ^3MC minimum, the complex passes through a ^3TS where both bonds of a single bipyridine ligand are dissociating symmetrically. After the ^3TS , the IRC moved out upon a sort of ridge in hyperspace from which it was found to be able to bifurcate to either of two symmetry-equivalent ^3MC valleys (i.e., minimum energy geometries). One would normally expect to be able to apply the Bell-Evans-Polanyi principle [61, 62] which predicts a linear relationship between the ^3TS - $^3\text{MLCT}$ barrier and the $^3\text{MLCT}$ - ^3MC energy difference. In particular, in the double parabola model described in Article **III**, the height of the ^3TS - $^3\text{MLCT}$ barrier should decrease as the $^3\text{MLCT}$ - ^3MC energy difference increased. However the Bell-Evans-Polanyi principle is not applicable in the case of the above mentioned bifurcation. In fact, we found that the ^3TS - $^3\text{MLCT}$ barrier is the same to within the accuracy of our numerical method.

The $^3\text{MLCT} \rightarrow ^3\text{MC}$ *trans*-dissociation reaction in CH_3CN is very different than in the gas phase. The polar nature of the CH_3CN solvent has two implications. The first is that the $^3\text{MLCT}$ minimum is stabilized relative to the ^3MC minimum. In fact, we find the $^3\text{MLCT}$ minimum to now have a lower energy than the ^3MC minimum, which is just the opposite of what was found in the gas phase. The second implication of the polar solvent is a symmetry breaking of the ^3TS for the $^3\text{MLCT} \rightarrow ^3\text{MC}$ *trans*-dissociation reaction. The ^3TS is stabilized by lowering its symmetry so that one of the bipyridine ligand bonds is now breaking faster than the other for the same ligand. These points are illustrated for complex **70** by the NEB results from ORCA shown in **Fig. 8** and the carefully optimized IRC results from GAUSSIAN shown in **Fig. 9**. (See the SI for the corresponding figures for complex **6**.) A little thought shows that this implies two routes to the same *trans*-dissociated product. The asymmetry of the TS in our implicit solvent calculation leads us to revise the cartoon shown in Fig. 6 of Article **III** and to replace it with the new cartoon shown in **Fig. 10**. As no bifurcation is observed and we may now expect that the Bell-Evans-Polanyi principle to apply.

3.4 LI3 Orbital-Based Luminescence Index

We have seen that the original definition of LI3 must be replaced with the new definition given by LI4 in the solution case, otherwise the values vary too much between gas and solvated molecules. But since LI4 in solution is essentially the same as the gas-phase LI3, we will continue to use our previously calculated values of LI3. Let us first review what we have already learned about LI3 from our previous gas-phase work. We will then discuss what is the same in our CH_3CN solution calculations and what is different than in our previous gas-phase calculations.

Article **II** proposed the LI3 orbital-based luminescence index as an estimate of the $^3\text{MLCT} \rightarrow ^3\text{MC}$ barrier and a good correlation was found between LI3 and a E_{ave} “barrier height” derived from the temperature-dependence of luminescence lifetimes of about 100 polypyridine Ru(II) complex condensed-phase measurements. This is not a proof that LI3 correlates directly with the real $^3\text{MLCT} \rightarrow ^3\text{MC}$ barrier height. Indeed Article **III** investigated the relationship between LI3 and the energetics of the $^3\text{MLCT} \rightarrow ^3\text{MC}$ *trans*-

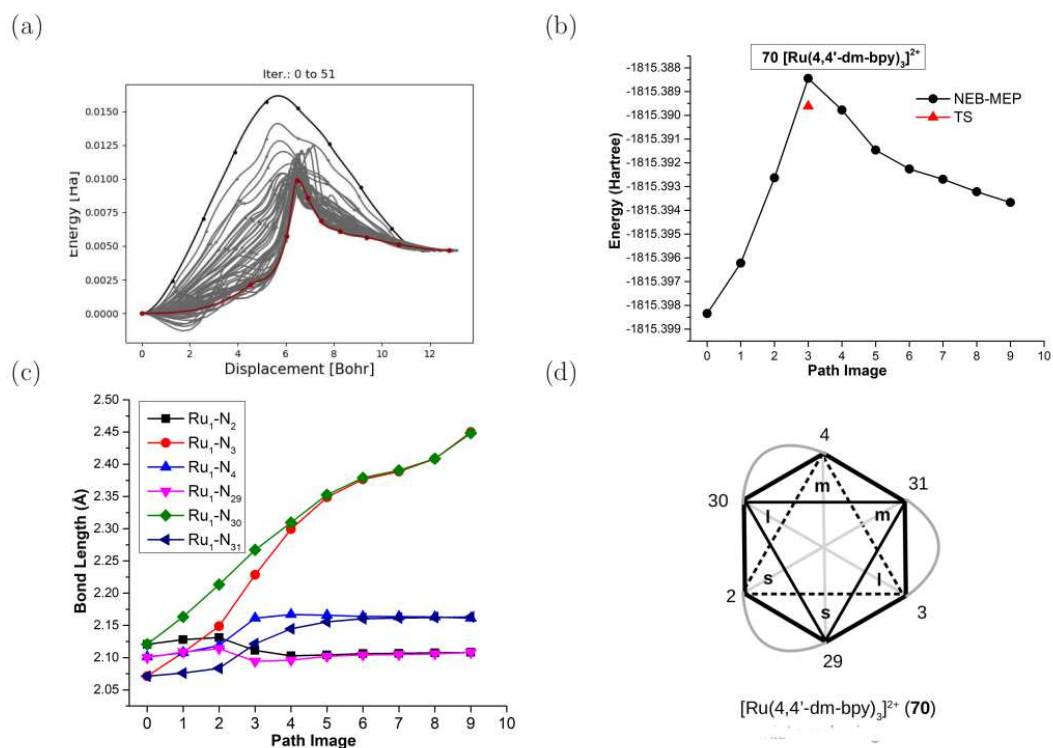


Figure 8: ${}^3\text{MLCT} \rightarrow {}^3\text{MC}$ NEB scan for complex **70** at the B3LYP(VWN3)/6-31G & LANL2DZ(Ru)/SMD(CH_3CN) level: (a) NEB iterations, (b) final NEB, (c) corresponding Ru-N bond distances along the NEB, and (d) cartoon of TS.

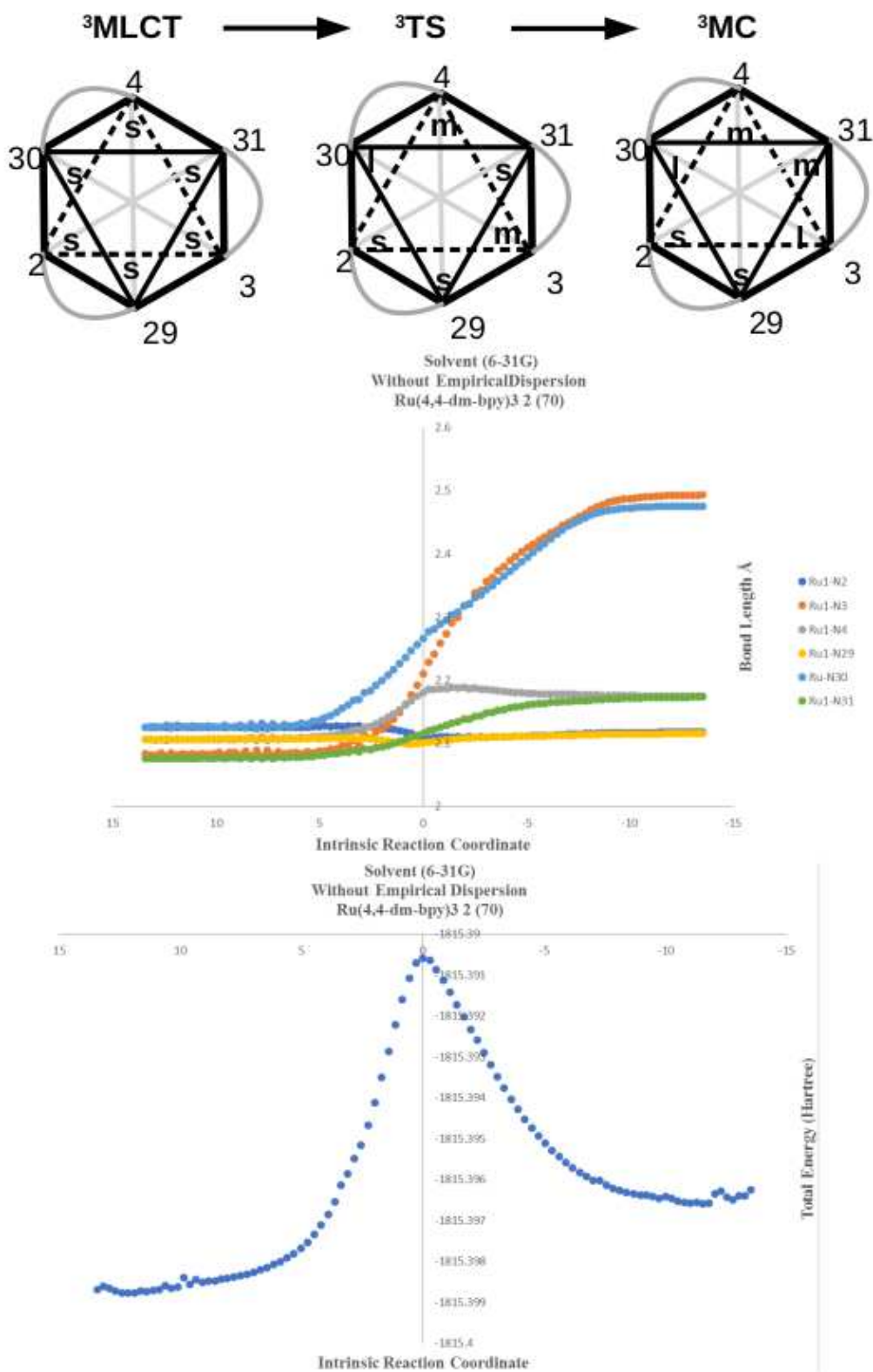


Figure 9: ${}^3\text{MLCT} \rightarrow {}^3\text{MC}$ IRC scan for complex **70** at the B3LYP(VWN3)/6-31G & LANL2DZ(Ru)/SMD(CH₃CN) level.

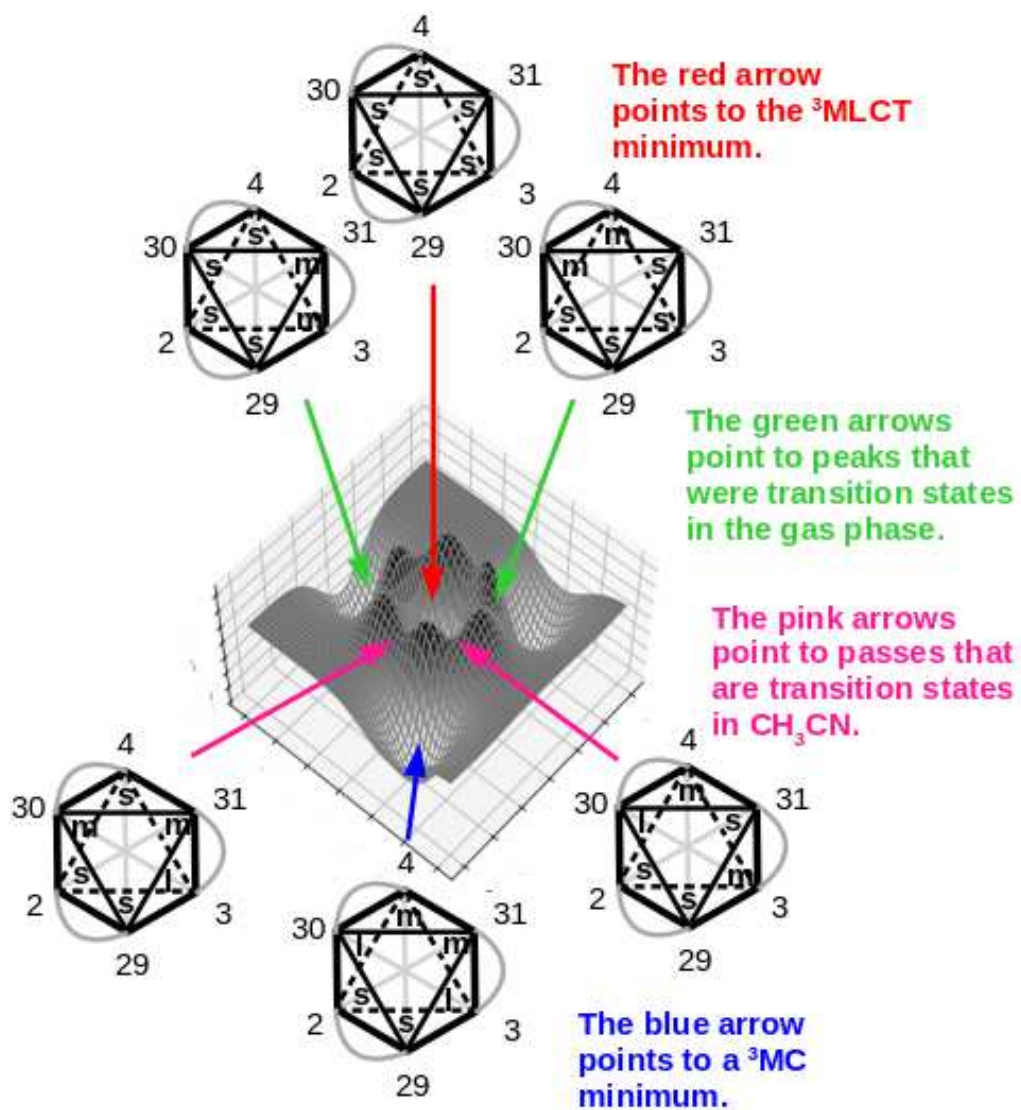


Figure 10: Cartoon showing our understanding of the main features of the triplet PES for complex 70.

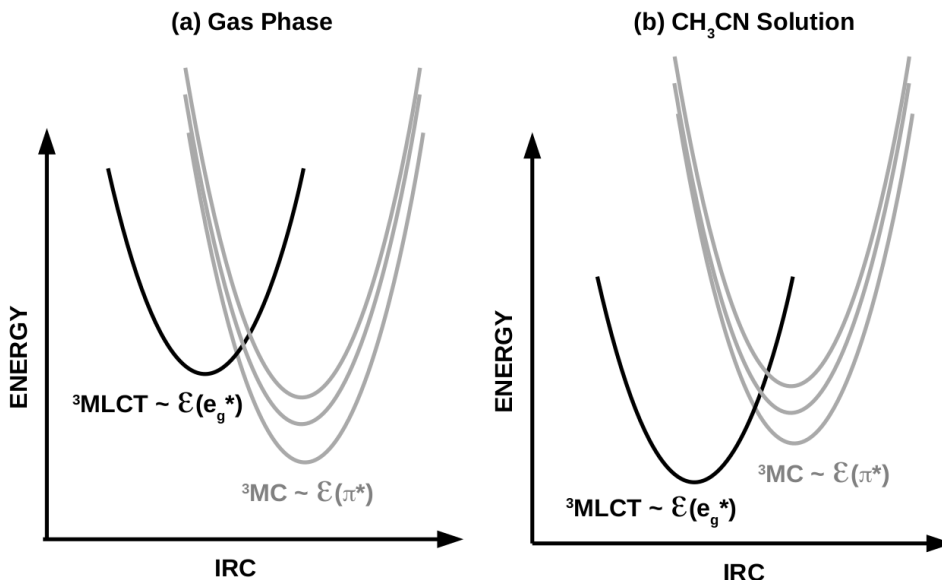


Figure 11: Naïve double parabola model. The position of the ${}^3\text{TS}$ is approximated as where the ${}^3\text{MLCT}$ and ${}^3\text{MC}$ curves cross. In either the gas-phase or in CH_3CN , increasing the ${}^3\text{MLCT}$ - ${}^3\text{MC}$ energy difference (i.e., making it less negative in the CH_3CN case) decreases the ${}^3\text{TS}$ - ${}^3\text{MLCT}$ energy difference (i.e., the ${}^3\text{MLCT} \rightarrow {}^3\text{MC}$ barrier height).

dissociation reaction in gas phase. In the gas phase, the ${}^3\text{MLCT}$ minimum was found to be at higher energy than that of the ${}^3\text{MC}$ minimum. It was found that the ${}^3\text{MLCT}$ - ${}^3\text{MC}$ energy difference increased as LI3 increased. This was explained in Article **III** by the use of a naïve double parabola model (**Fig. 11**) with the energies of the products (P) and reactants (R) at the reactant geometry (x_R) given by,

$$\begin{aligned} E_P(x_R) &\approx \epsilon_{\pi^*} \\ E_R(x_R) &\approx \epsilon_{e_g^*}, \end{aligned} \quad (4)$$

relative to the energy of the $(t_{2g})^5(\pi^*)^0(e_g^*)^0$ configuration. Then

$$\text{LI3} = \frac{[(E_P(x_R) + E_R(x_R))/2]^2}{E_P(x_R) - E_R(x_R)}. \quad (5)$$

[The plus and minus signs were accidentally interchanged in Article **III**. See Eq. (4) of that article.] This shows that increasing LI3 is mainly due to decreasing $E_P(x_R) - E_R(x_R)$ which translates to decreasing the ${}^3\text{MC}$ - ${}^3\text{MLCT}$ energy difference or, equivalently, to increasing the ${}^3\text{MLCT}$ - ${}^3\text{MC}$ energy difference.

Figure 12 shows that the ${}^3\text{MLCT}$ - ${}^3\text{MC}$ energy difference increases as LI3 increases, just as it does in the gas phase (compare with Fig. 15 of Article **III**). The only new thing in CH_3CN is that this energy difference is now negative rather than positive. As explained above, the absence of a bifurcation on the *trans* ${}^3\text{MLCT} \rightarrow {}^3\text{MC}$ pathway suggests that the Bell-Evans-Polanyi principle should apply so that we should see a linear relationship between the ${}^3\text{TS}$ - ${}^3\text{MLCT}$ barrier height and both the ${}^3\text{MLCT}$ - ${}^3\text{MC}$ energy difference and LI3. As explained above, the two parabola model predicts that the slope of the graphs should be negative. This is confirmed in **Fig. 13** at the B3LYP(VWN3)/6-31G

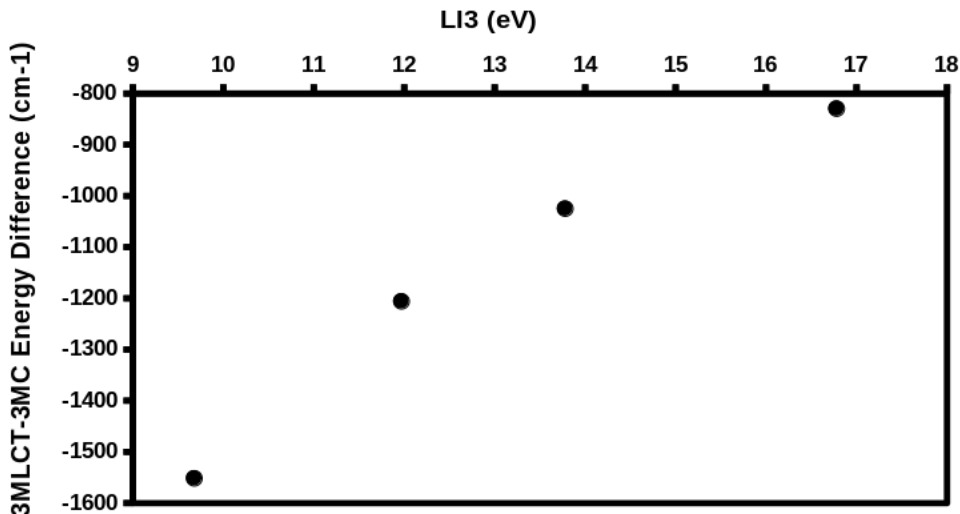


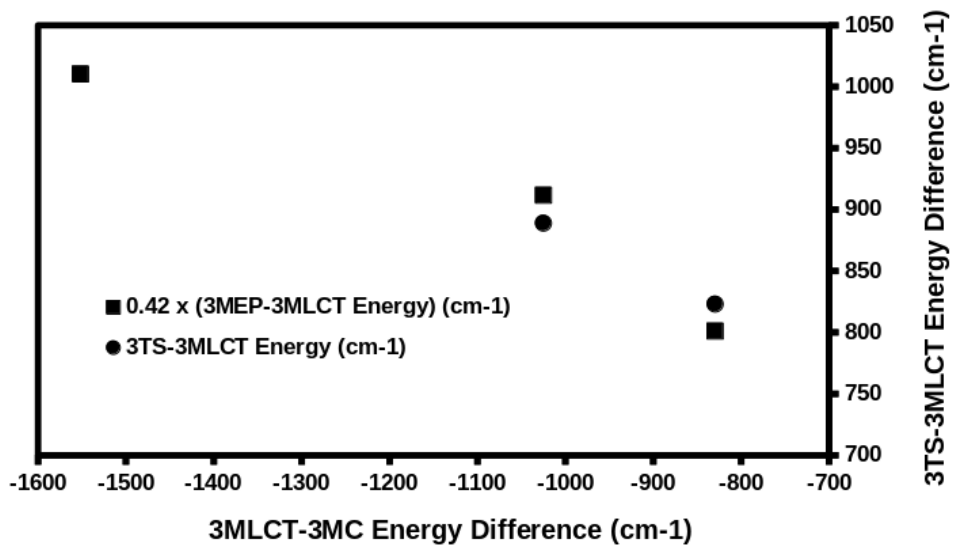
Figure 12: Variation of the ${}^3\text{MLCT}$ - ${}^3\text{MC}$ energy difference calculated at the B3LYP(VWN3)/6-31G & LANL2DZ(Ru)/SMD(CH_3CN) level as a function of LI3.

& LANL2DZ(Ru)/SMD(CH_3CN) level of calculation. Note that due to computational resource and time limitations, we have only managed to converge two transition states. However we have also included scaled values of the maximum energy points (${}^3\text{MEP}$) along the NEB as an estimate of the ${}^3\text{TS}$ values.

As discussed above, the orbital-based LI3 luminescence index was designed as a qualitative measure of the ${}^3\text{TS}$ - ${}^3\text{MLCT}$ barrier height. However the gas-phase calculations in Article **III** and the present CH_3CN implicit solvent calculations indicate that the ${}^3\text{TS}$ - ${}^3\text{MLCT}$ barrier height actually decreases as LI3 increases. This is at odds with the traditional explanation of luminescence in ruthenium(II) polypyridine complexes. The question is now, “Why?”

The short answer is that photochemical kinetic models involve many choices and assumptions (e.g., Is the mechanism better described by Marcus charge transfer theory or by Eyring transition state theory and does temperature even make sense in this context?) A longer and very interesting answer has been given by Hernández-Castillo, Eder, and González [13] in a recent review which emphasizes the need to take competing pathways into account in order to give a quantitative explanation of luminescence lifetimes in these compounds. To some extent, this has been apparent for some time (e.g., see the elaborate model of luminescence lifetimes discussed in Article **II** before drastic simplification). Interestingly Hernández-Castillo, Eder, and González suggest that the main pathway for luminescence quenching is by whichever pathway leads most quickly back to the ground state and that this is *not* the traditional *trans* dissociation mechanism. At the risk of oversimplification, we suggest that our results are consistent with the idea that the *trans* dissociation ${}^3\text{MLCT} \rightarrow {}^3\text{MC}$ mechanism may be serving as a reservoir for repopulating the phosphorescent ${}^3\text{MLCT}$ state and therefore that luminescence lifetimes will actually increase as the *trans* dissociation ${}^3\text{MLCT} \rightarrow {}^3\text{MC}$ barrier height decreases.

(a)



(b)

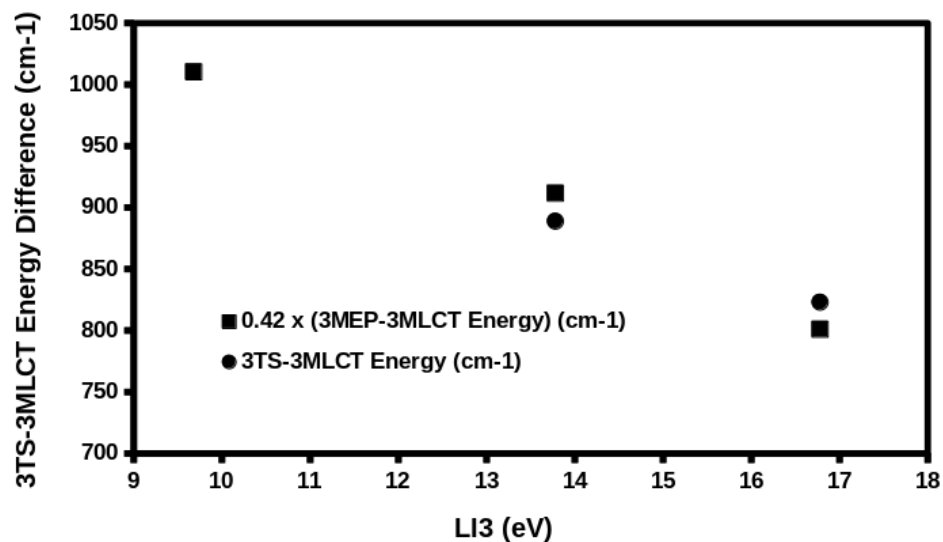


Figure 13: Applicability of the Bell-Evans-Polanyi principle to *trans* dissociation on the triplet B3LYP(VWN3)/6-31G & LANL2DZ(Ru)/SMD(CH₃CN) PES. Barrier height as a function of: (a) ³MLCT-³MC Energy Difference, (b) LI3. Here MEP refers to the maximum energy point along the NEB. This is typically an overestimate of the TS, so we have taken the liberty of scaling the ³MEP-³MLCT energy difference by a factor of 0.42.

4 Conclusion

Mixed quantum/classical (and sometimes completely quantum) photodynamics modeling represents a state-of-the-art technique for investigating photoprocesses such as luminescence in ruthenium(II) polypyridine complexes. However these more sophisticated techniques suffer not only from their heavy use of computational resources, making applications to luminescence in ruthenium(II) polypyridine complexes extraordinarily rare, but they are also far removed from the ligand-field theory (LFT) orbital-based thinking common among most synthetic chemists. We have tried to remedy this failure in a series of papers (**I** [14], **II** [15], **III** [16]) of which the present paper is Article **IV**. In particular, Article **II** showed that the third orbital-based luminescence index (LI3) that we developed based upon the use of frontier-molecular orbital factors that we expected would govern the ${}^3\text{MLCT} \rightarrow {}^3\text{MC}$ *trans*-dissociation barrier height and computed using the partial density of states (PDOS) method of Article **I** correlated well with experimentally-derived trends in the ${}^3\text{MLCT} \rightarrow {}^3\text{MC}$ *trans*-dissociation barrier height. However correlation is not causality and so we sought a deeper explanation of what the LI3 index was actually measuring. Article **III** studied the gas-phase ${}^3\text{MLCT} \rightarrow {}^3\text{MC}$ *trans*-dissociation mechanism. It was found that the barrier height was ligand-independent to within the accuracy of our computations but that LI3 correlates well with the energy difference between the higher-energy ${}^3\text{MLCT}$ state and the lower-energy ${}^3\text{MC}$ state. Although the Bell-Evans-Polanyi principle would normally imply that the barrier height should also correlate with LI3, this was not so because of a novel pathway involving charge transfer to a single bipyridine ligand which symmetrically distances itself from the metal atom before then bifurcating to one of two isomers. For this same reason, the transition state is particularly hard to converge.

As most experimental measurements of luminescence lifetimes are done for complexes in condensed phases, it was felt that it was particularly important to carry out calculations for the solution phase reaction. This article reports these calculations obtained in CH_3CN using an implicit solvent model. Several things differences between the gas-phase and CH_3CN solution mechanisms. The solvent stabilizes the ${}^3\text{MLCT}$ state so that it is now *lower in energy* than the ${}^3\text{MC}$ state. It also has the effect of polarizing the ${}^3\text{MLCT} \rightarrow {}^3\text{MC}$ *trans*-dissociation transition state (${}^3\text{TS}$) so that each gas-phase ${}^3\text{TS}$ becomes two ${}^3\text{TS}$ s in solution. This eliminates the bifurcation, making convergence of the ${}^3\text{TS}$ easier except that the solvent model requires additional computational resources. The solvent also shifts the PDOS but does not change its shape, so that we may replace the LI3 luminescence index with a new LI4 luminescence index which is insensitive to the presence of the solvent and less sensitive to the choice of functional and basis set. The LI4 luminescence index also correlates well with both the ${}^3\text{MC}$ - ${}^3\text{MLCT}$ energy difference and, consistent with the Bell-Evans-Polanyi prediction, with the corresponding barrier height.

Surprisingly, the longest luminescence lifetimes are found to be associated with the *lowest* barrier heights, rather than with the highest barrier heights as previously believed. To be fair, photochemical rate theory is not as well understood as thermal (i.e., ground-state) rate theory. It is far from obvious what temperature means for photochemical processes when applying Eyring transition state theory or whether we are in a recrossing regime where Marcus charge transfer theory should apply or whether we might instead be in some intermediate or perhaps even new type of regime. Hernández, Eder, and González

recently summarized the relevant literature for the theory of luminescence lifetimes in ruthenium(II) polypyridine complexes and presented a new, more complete, theory [13]. At the risk of oversimplification of their theory, we will summarize it by saying that luminescence quenching occurs not by reaching the ^3MC state but by a rapid return to the singlet ground state by another route. If we believe that this, then it might mean that a lower *trans* barrier leads to a *longer* luminescence lifetime by preventing the molecule from finding the most efficient route to return to the ground state. Of course, we must caution that much more investigation needs to be done before we can be confident in our model for the overall global mechanism governing luminescence lifetimes, even in the limited class of complexes constituted by ruthenium(II) polypyridine complexes.

Supplementary Information

Only plots for complex **70** have been used in the main article. Among other supplementary information are some plots for other complexes.

1. Comparison of GAUSSIAN and ORCA results
2. PDOS
3. Contour plots
4. *Trans* dissociation TSs and IRCs
5. Author contributions

Acknowledgement

DM and MEC gratefully acknowledge helpful funding from the African School on Electronic Structure Methods and Applications (ASESMA), ASESMANet, and the US-Africa Initiative. We are indebted to a number of people for insightful discussions throughout our studies of orbital-based luminescence indices in ruthenium(II) polypyridine complexes. Many of these people have already been thanked in Article **III** [16] and we, though we are grateful, will not repeat the list of names here. Instead, we would like to take this opportunity to thank members of the ORCA team for helping us to understand what options are needed to obtain the best possible agreement between ORCA and GAUSSIAN calculations. In particular, we are indebted to Miquel Garcia Rates, Frank Neese, Christoph Riplinger, Georgi Stoychev, and Frank Wennmohs for helpful discussions about subtle aspects of numerical algorithms used in the present article. We would like to thank Pierre Girard and Sébastien Morin for technical support in the context of the Grenoble *Centre d'Experimentation du Calcul Intensif en Chimie (CECIC)* computers used for the calculations reported here.

Author Information

Corresponding Author

Ala Aldin M. H. M. Darghouth*
College of Sciences, University of Mosul, Al Majmoaa Street, Mosul, 41002
Iraq
E-mail: aladarghouth@uomosul.edu.iq

Authors

Denis Magero
School of Science, Technology and Engineering, Department of Chemistry and
Biochemistry, Alupe University, P.O. Box 845-50400, Busia, Kenya
E-mail: dmagero@au.ac.ke

Mark E. Casida
Laboratoire de Spectrométrie, Interactions et Chimie théorique (SITh), Département
de Chimie Moléculaire (DCM, UMR CNRS/UGA 5250), Institut de Chimie
Moléculaire de Grenoble (ICMG, FR2607), Université Grenoble Alpes (UGA)
301 rue de la Chimie, BP 53, F-38041 Grenoble Cedex 9, France
orcid.org/0000-0002-9124-0530;
E-mail: mark.casida@univ-grenoble-alpes.fr

References

- [1] D. Magero, T. Mestiri, K. Alimi, and M. E. Casida, [Computational studies of ruthenium and iridium complexes for energy sciences and progress on greener alternatives](#), in *Green Chemistry and Computational Chemistry: Shared Lessons in Sustainability*, edited by L. Mammimo, pages 115–145, Elsevier, 2020, preprint: <https://arxiv.org/abs/2004.03345>.
- [2] J. P. Sauvage, J. P. Collin, J. C. Chambron, S. Guillerez, and C. Coudret, [Ruthenium\(II\) and osmium\(II\) bis\(terpyridine\) complexes in covalently-linked multicomponent systems: Synthesis, electrochemical behavior, absorption spectra, and photochemical and photophysical properties](#), *Chem. Rev.* **94**, 993 (1994).
- [3] K. Nakamaru, [Synthesis, luminescence quantum yields, and lifetimes of trischelated ruthenium \(II\) mixed-ligand complexes including 3,3'-dimethyl-2,2'-bipyridyl](#), *Bull. Chem. Soc. Jpn.* **55**, 2697 (1982).
- [4] G. Liebsch, I. Klimant, and O. S. Wolfbeis, [Luminescence lifetime temperature sensing based on sol-gels and poly\(acrylonitrile\)s dyed with ruthenium metal-ligand complexes](#), *Adv. Mat.* **11**, 1296 (1999).
- [5] V. Balzani and A. Juris, [Photochemistry and photophysics of Ru \(II\) polypyridine complexes in the Bologna group. From early studies to recent developments](#), *Coordin. Chem. Rev.* **211**, 97 (2001).
- [6] M. Duati, S. Tasca, F. C. Lynch, H. Bohlen, J. G. Vos, S. Stagni, and M. D. Ward, [Enhancement of luminescence lifetimes of mononuclear ruthenium\(II\)-terpyridine complexes by manipulation of the \$\sigma\$ -donor strength of ligands](#), *J. Inorg. Chem.* **42**, 8377 (2003).

- [7] A. Harriman, A. Khatyr, and R. Ziessel, [Extending the luminescence lifetime of ruthenium\(II\) poly\(pyridine\) complexes in solution at ambient temperature](#), Dalton Trans. **10**, 2061 (2003).
- [8] E. A. Medlycott and G. S. Hanan, [Designing tridentate ligands for ruthenium\(II\) complexes with prolonged room temperature luminescence lifetimes](#), Chem. Soc. Rev. **34**, 133 (2005).
- [9] L. J. Nurkkala, R. O. Steen, H. K. J. Friberg, J. A. Häggström, P. V. Bernhardt, M. J. Riley, and S. J. Dunne, [The effects of pendant vs. fused thiophene attachment upon the luminescence lifetimes and electrochemistry of tris\(2,2'-bipyridine\)ruthenium\(II\) complexes](#), Eur. J. Inorg. Chem. **26**, 4101 (2008).
- [10] S. Ji, W. Wu, W. Wu, P. Song, K. Han, Z. Wang, S. Liu, H. Guo, and J. Zhao, [Tuning the luminescence lifetimes of ruthenium\(II\) polypyridine complexes and its application in luminescent oxygen sensing](#), J. Mater. Chem. **20**, 1953 (2010).
- [11] A. Soupart, F. Alary, J. Heully, P. I. P. Elliot, and I. M. Dixon, [Theoretical study of the full photosolvolytic mechanism of \$\[\text{Ru}\(\text{bpy}\)_3\]^{2+}\$: Providing a general mechanistic roadmap for the photochemistry of \$\[\text{Ru}\(\text{N}\wedge\text{N}\)_3\]^{2+}\$ -type complexes toward both cis and trans photoproducts](#), Inorg. Chem. **59**, 14679 (2020).
- [12] V. Balzani, P. Ceroni, A. Credi, and M. Venturi, [Ruthenium tris\(bipyridine\) complexes: Interchange between photons and electrons in molecular-scale devices and machines](#), Coord. Chem. Rev. **433**, 213758 (2021).
- [13] D. Hernández-Castillo, I. Eder, and L. González, [Guidelines to calculate non-radiative deactivation mechanisms of ruthenium tris\(bipyridine\) derivatives](#), Coord. Chem. Rev. **510**, 215819 (2024).
- [14] C. M. Wawire, D. Jouvenot, F. Loiseau, P. Baudin, S. Liatard, L. Njenga, G. Kamau, and M. E. Casida, [Density-functional study of luminescence in polypyridine ruthenium complexes](#), J. Photochem. and Photobiol. A **276**, 8 (2014).
- [15] D. Magero, M. E. Casida, G. Amolo, N. Makau, and L. Kituyi, [Partial density of states ligand field theory \(PDOS-LFT\): Recovering a LFT-like picture and application to photoproperties of ruthenium\(II\) polypyridine complexes](#), J. Photochem. Photobiol. A **348**, 305 (2017).
- [16] D. Magero, A. M. H. M. Dargouth, and M. Casida, [Test of the orbital-based LI3 index as a predictor of the height of the \${}^3\text{MLCT} \rightarrow {}^3\text{MC}\$ transition-state barrier for gas-phase \$\[\text{Ru}\(\text{N}\wedge\text{N}\)_3\]^{2+}\$](#) , J. Photochem. Photobiol. A: Chem. **451**, 115502 (2024).
- [17] I. B. Bersuker, [Modern aspects of the jahn-teller effect theory and applications to molecular problems](#), Chem. Rev. **101**, 1067 (2001).
- [18] I. Bolaño Losada and P. Persson, [Ligand-centered to metal-centered activation of a Rh\(III\) photosensitizer revealed by *ab initio* molecular dynamics simulations](#), Chem. Sci. **14**, 13713 (2023).

- [19] J. Condradie, [Effect of density functional approximations on the calculated Jahn-Teller distortion in bis\(terpyridine\)manganese\(III\) and related compounds](#), *J. Molec. Modeling* **30**, 20 (2024).
- [20] I. Tavernelli, B. R. E. Curchod, , and U. Rothlisberger, [Nonadiabatic molecular dynamics with solvent effects: A LR-TDDFT QM/MM study of ruthenium \(II\) tris \(bipyridine\) in water](#), *Chem. Phys.* **391**, 101 (2011).
- [21] L. G. Vanquickenborne and A. Ceulemans, [Ligand-field models and the photochemistry of coordination compounds](#), *Coord. Chem. Rev.* **48**, 157 (1983).
- [22] M. J. Frisch et al., [Gaussian 09 Revision D.01](#), Gaussian Inc. Wallingford CT 2009.
- [23] F. Neese, F. Wennmohs, U. Becker, and C. Riplinger, [The ORCA quantum chemistry program package](#), *J. Chem. Phys.* **152**, 224108 (2020).
- [24] P. J. Stephens, F. J. Devlin, C. F. Chabalowski, and M. J. Frisch, [Ab initio calculation of vibrational absorption and circular dichroism spectra using density functional force fields](#), *J. Phys. Chem.* **98**, 11623 (1994).
- [25] S. H. Vosko, L. Wilk, and M. Nusair, [Accurate spin-dependent electron liquid correlation energies for local spin density calculations: a critical analysis](#), *Can. J. Phys.* **58**, 1200 (1980).
- [26] J. Tomasi and M. Persico, [Molecular interactions in solution: an overview of methods based on continuous distributions of the solvent](#), *Chem. Rev.* **94**, 2027 (1994).
- [27] C. J. Cramer and D. G. Truhlar, [Implicit solvation models: equilibria, structure, spectra, and dynamics](#), *Chem. Rev.* **99**, 2161 (1999).
- [28] J. Tomasi, B. Mennucci, and R. Cammi, [Quantum mechanical continuum solvation models](#), *Chem. Rev.* **105**, 2999 (2005).
- [29] A. V. Marenich, C. J. Cramer, and D. G. Truhlar, [Universal solvation model based on solute electron density and on a continuum model of the solvent defined by the bulk dielectric constant and atomic surface tensions](#), *J Phys Chem B* **113**, 6378 (2009).
- [30] A. Soupart, I. M. Dixon, F. Alary, and J. Heully, [DFT rationalization of the room-temperature luminescence properties of Ru\(bpy\)₃²⁺ and Ru\(tpy\)₃²⁺: ³MLCT-³MC minimum energy path from neb calculations and emission spectra from vres calculations](#), *Theor. Chem. Acc.* **137**, 37 (2018).
- [31] E. Lebon, S. Bastin, P. Sutra, L. Vendier, R. E. Piau, I. M. Dixon, M. Boggio-Pasqua, F. Alary, J. L. Heully, A. Igau, and A. Juris, [Can a functionalized phosphine ligand promote room temperature luminescence of the \[Ru\(bpy\)\(tpy\)\]²⁺ core?](#), *Chem. Comm.* **48**, 741 (2012).
- [32] I. M. Dixon, J. Heully, F. Alary, and P. I. P. Elliott, [Theoretical illumination of highly original photoreactive ³MC states and the mechanism of the photochemistry of Ru\(II\) tris\(bidentate\) complexes](#), *Phys. Chem. Chem. Phys.* **19**, 27765 (2017).

- [33] A. Soupart, F. Alary, J. Heully, P. I. P. Elliott, and I. M. Dixon, [Exploration of the uncharted \$^3\text{PES}\$ territory for \$\[\text{Ru}\(\text{bpy}\)_3\]^{2+}\$ A new \$^3\text{MC}\$ minimum prone to ligand loss photochemistry](#), *Inorg. Chem.* **57**, 3192 (2018).
- [34] R. Ditchfield, W. Hehre, and J. A. Pople, [Self-consistent molecular-orbital methods. IX. An extended Gaussian-type basis for molecular-orbital studies of organic molecules](#), *J. Chem. Phys.* **54**, 724 (1971).
- [35] W. J. Hehre, R. Ditchfield, and J. A. Pople, [Self—consistent molecular orbital methods. XII. Further extensions of gaussian—type basis sets for use in molecular orbital studies of organic molecules](#), *J. Chem. Phys.* **56**, 2257 (1972).
- [36] P. J. Hay and W. R. Wadt, [Ab initio effective core potentials for molecular calculations. potentials for K to Au including the outermost core orbitals](#), *J. Chem. Phys.* **82**, 299 (1985).
- [37] F. Weigend and R. Ahlrichs, [Balanced basis sets of split valence, triple zeta valence and quadruple zeta valence quality for H to Rn: Design and assessment of accuracy](#), *Phys. Chem. Chem. Phys.* **7**, 3297 (2005).
- [38] D. Andrae, U. Haeussermann, M. Dolg, and H. Preuß, [Energy-adjusted ab initio pseudopotentials for the second and third row transition elements](#), *Theor. Chim. Acta* **77**, 123 (1990).
- [39] D. Andrae, U. Häußermann, M. Dolg, H. Stoll, and M. Preuß, [Energy-adjusted ab initio pseudopotentials for the second and third row transition elements: molecular test for \$\text{M}_2\$ \(\$\text{M} = \text{Ag}, \text{Au}\$ \) and \$\text{MH}\$ \(\$\text{M} = \text{Ru}, \text{Os}\$ \)](#), *Theor. Chim. Acta* **78**, 247 (1991).
- [40] S. Grimme, J. Antony, S. Ehrlich, and H. Krieg, [A consistent and accurate ab initio parametrization of density functional dispersion correction \(DFT-D\) for the 94 elements H-Pu](#), *J. Chem. Phys.* **132**, 154104 (2010).
- [41] S. Grimme, S. Ehrlich, and L. Goerigk, [Effect of the damping function in dispersion corrected density functional theory](#), *J. Comput. Chem.* **32**, 1456 (2011).
- [42] R. Ketkaew, [GAUSSIAN: Use B3LYP-VWN5 instead of B3LYP-VWN3](#), <https://sites.google.com/site/rangsiman1993/comp-chem/tips-and-tricks/gaussian-b3lyp>, last accessed 6 March 2024.
- [43] E. Cancès, B. Mennucci, and J. Tomasi, [A new integral equation formalism for the polarizable continuum model: Theoretical background and applications to isotropic and anisotropic dielectrics](#), *J. Chem. Phys.* **107**, 3032 (1997).
- [44] B. Mennucci, E. Cancès, and J. Tomasi, [Evaluation of solvent effects in isotropic and anisotropic dielectrics and in ionic solutions with a unified integral equation method: Theoretical bases, computational implementation, and numerical applications](#), *J. Phys. Chem. B* **101**, 10506 (1997).
- [45] B. Mennucci and J. Tomasi, [Continuum solvation models: A new approach to the problem of solute's charge distribution and cavity boundaries](#), *J. Chem. Phys.* **106**, 5151 (1997).

- [46] J. Tomasi, B. Mennucci, and E. Cancès, [The IEF version of the PCM solvation method: an overview of a new method addressed to study molecular solutes at the QM *ab initio* level](#), J. Mol. Struct. (Theochem) **464**, 211 (1999).
- [47] A. Klamt and G. Schüürmann, [COSMO: a new approach to dielectric screening in solvents with explicit expressions for the screening energy and its gradient](#), J. Chem. Soc., Perkin Trans. **2**, 799 (1993).
- [48] T. N. Truong and E. V. Stefanovich, [A new method for incorporating solvent effect into the classical, *ab initio* molecular orbital and density functional theory frameworks for arbitrary shape cavity](#), Chem. Phys. Lett. **240**, 253 (1995).
- [49] K. Baldrige and A. Klamt, [First principles implementation of solvent effects without outlying charge error](#), J. Chem. Phys. **106**, 6622 (1997).
- [50] V. Barone and M. Cossi, [Quantum calculation of molecular energies and energy gradients in solution by a conductor solvent model](#), J. Phys. Chem. A **102**, 1995 (1998).
- [51] M. Cossi, N. Rega, G. Scalmani, and V. Barone, [Energies, structures, and electronic properties of molecules in solution with the C-PCM solvation model](#), J. Comput. Chem. **24**, 669 (2003).
- [52] L. N. Gregerson and K. K. Baldrige, [Outlying charge, stability, efficiency, and algorithmic enhancements in the quantum-mechanical solvation method, COSab-GAMESS](#), Helv. Chim. Acta **86**, 4112 (2003).
- [53] B. Ginovska, D. M. Camaioni, M. Dupuis, C. A. Schwerdtfeger, and Q. Gil, [Charge-dependent cavity radii for an accurate dielectric continuum model of solvation with emphasis on ions: Aqueous solutes with oxo, hydroxo, amino, methyl, chloro, bromo, and fluoro functionalities](#), J. Phys. Chem. A **112**, 10604 (2008).
- [54] R. Krishnan, J. S. Binkley, R. Seeger, and J. A. Pople, [Self-consistent molecular orbital methods. XX. A basis set for correlated wave functions](#), J. Chem. Phys. **72**, 650 (1980).
- [55] K. Lin, Q. Li, R. Yu, J. Chen, J. P. Attfield, and X. Xing, [Chemical pressure in functional materials](#), Chem. Soc. Rev. **51**, 5351 (2022).
- [56] M. Wolfsberg and L. J. Helmholz, [The spectra and electronic structure of the tetrahedral ions \$\text{MnO}_4^-\$, \$\text{CrO}_4^{2-}\$, and \$\text{ClO}_4^-\$](#) , J. Chem. Phys. **20**, 837 (1952).
- [57] Q. Sun, B. Dereka, E. Vauthey, L. M. L. Daku, and A. Hauser, [Ultrafast transient IR spectroscopy and DFT calculations of ruthenium\(II\) polypyridyl complexes](#), Chem. Sci. **8**, 223 (2017).
- [58] J. V. Caspar and T. J. Meyer, [Photochemistry of *tris*\(2,2'-bipyridine\) ruthenium\(ii\) ion \(\$\[\text{Ru}\(\text{bpy}\)_3\]^{2+}\$ \). Solvent effects.](#), J. Am. Chem. Soc. **105**, 5583 (1983).
- [59] A. Fouqueau, S. Mer, M. E. Casida, L. M. Lawson Daku, A. Hauser, T. Mineva, and F. Neese, [Comparison of density functionals for energy and structural differences between the high \$\[^5T_{2g} : \(t_{2g}\)^4\(e_g\)^2\]\$ and low \$\[^1A_{1g} : \(t_{2g}\)^6\(e_g\)^0\]\$ spin states of the hexaquoferrous cation, \$\[\text{Fe}\(\text{H}_2\text{O}\)_6\]^{2+}\$](#) , J. Chem. Phys. **120**, 9473 (2004).

- [60] A. Fouqueau, M. E. Casida, L. M. Lawson Daku, A. Hauser, and F. Neese, [Comparison of density functionals for energy and structural differences between the high \$\[^5T_{2g} : \(t_{2g}\)^4\(e_g\)^2\]\$ and low \$\[^1A_{1g} : \(t_{2g}\)^6\(e_g\)^0\]\$ spin states of iron\(II\) coordination compounds: II. More functionals and the hexaminoferrous cation, \$\[\text{Fe}\(\text{NH}_3\)_6\]^{2+}\$](#) , J. Chem. Phys. **122**, 044110 (2005).
- [61] R. P. Bell, [The theory of reactions involving proton transfers](#), Proc. R. Soc. London, Ser. A **154**, 414 (1936).
- [62] M. G. Evans and M. Polanyi, [Further considerations on the thermodynamics of chemical equilibria and reaction rates](#), J. Chem. Soc., Faraday Trans. **32**, 1333 (1936).